How L34V mutation affect the structure, dynamics and aggregation of amyloid-β_{40} ($A\beta_{40}$) peptide: Key insights from molecular dynamics simulations

Thesis

Submitted for the fulfilment of the Degree

of

Master of Science

By

Hema Thakur

(Registration No: 301602021)

Under the guidance of

Dr. Bhupesh Goyal

Assistant Professor

School of Chemistry and Biochemistry

School of Chemistry and Biochemistry
Thapar Institute of Engineering and Technology (Deemed to be University)
Patiala-147004, Punjab (India)
www.thapar.edu

(June 30, 2018)

Certificate

This is to certify that the dissertation entitled **"*How L34V mutation affect the structure, dynamics and aggregation of amyloid-β$_{40}$ (Aβ$_{40}$) peptide: Key insights from molecular dynamics simulations*"** being submitted by Miss Hema Thakur to School of Chemistry and Biochemistry, Thapar Institute of Engineering and Technology, Patiala in partial fulfilment of the requirements for the award of degree of **Master of Science in Chemistry,** is an authentic record of bonafide work carried out by her under my guidance and supervision. She has fulfilled the requirements for the submission of this thesis, which to my knowledge has reached the requisite standard.

The results embodied in the thesis have not been submitted in part or full to any other University or Institute for the award of any degree or diploma.

Bhupesh Goyal
(Dr. Bhupesh Goyal)
Assistant Professor
School of Chemistry and Biochemistry
TIET, Patiala

Acknowledgements

I would like to express my heartfelt and sincere gratitude to Dr. Bhupesh Goyal, Assistant Professor, School of Chemistry and Biochemistry, for giving me the opportunity to work on this exhilarating and innovative project. I would also like to thank him for his inspiring guidance and valuable discussion throughout the course of my project work. We thank Dr. Deepti Goyal, Assistant Professor, Department of Chemistry, Sri Guru Granth Sahib World University, Fatehgarh Sahib for providing access to the computational facilities.

I wish to thank the Ph.D. scholars Miss Rajneet Kaur Saini, Mrs Suniba Shuaib and Mr Simranjeet Singh for their guidance and unremitting encouragement. I would also like to extend my thanks to Miss Diksha Sharma, Mr Rakesh Kumar, Mr Kartik Sharma, Mr Shantanu Aggarawal, Mr Anurag yadav and Mr Akhil Sharma for helping me throughout my project.

I would like to thank all my lab mates for their constant encouragement. I have no words to express my gratitude to my family members whose constant support and blessings have helped me to carry out this project.

Hema Thakur

Abstract

Alzheimer's disease (AD) is a neurodegenerative disease identified by Alois Alzheimer in 1907. AD is characterized by short-term memory loss, disorientation and impairment of judgement. According to amyloid cascade hypothesis, the aggregation of a 39-42 amino acid long peptide, amyloid-β (Aβ) peptide in brain is a major cause of AD. The recent studies demonstrated that L34V mutation changes the lethality, and rate of fibril formation of the wild type (wt) $A\beta_{40}$ peptide. However, the molecular mechanism behind increase in the wt $A\beta_{40}$ aggregation on L34V mutation remains unclear. In this regard, the influence of L34V mutation on the structure and dynamics of $A\beta_{40}$ was investigated using all-atom molecular dynamics simulations. The $A\beta_{40}$ monomer simulations starting from a random coil conformation highlight that L34V mutation cause noticeable changes in the conformational ensemble as well as in the secondary structure of the $A\beta_{40}$ peptide. The present investigation provides key physical insights into the increased rate of fibril formation upon L34V mutation and a detail atomistic picture of the L34V induced conformational changes in the wt $A\beta_{40}$.

Table of Contents

		Page No.
	Certificate	ii
	Acknowledgement	iii
	Abstract	iv
	Table of contents	v
	List of Tables	vi
	List of Figures	vii
	List of Abbreviations	ix
Chapter 1:	Introduction	1-18
1.1	Protein Folding	1
1.2	Protein Misfolding	3
1.3	Origin And Prevalence of Alzheimer Disease	4
1.4	Alzheimer's Symptomatology	6
1.5	Genesis of Alzheimer	8
1.6	Therapeutic Pathways For AD	13
1.7	Importance of Molecular Docking And Dynamics	14
1.8	Control Measures	15
1.9	Medication For AD	16
1.10	Objective of The Thesis	17
1.11	Overview of Thesis	18
Chapter 2 :	Literature Review	19-33
Chapter 3 :	Computational Details	34-36
Chapter 4 :	Results and Discussion	37-44
Chapter 5 :	Conclusions	45
References		46-52

List of Tables

Table number	Title	Page number
1	Summary of the mutations	31
2	The total number of microstates and the percentage population of five most-populated microstates (**m_1**, **m_2**, **m_3**, **m_4** and **m_5**) of $A\beta_{40}$ and $A\beta_{40}$(L34V) during MD simulation in explicit water.	39
3	Statistical representation of secondary structure components of $A\beta_{40}$ and $A\beta_{40}$(L34V) during molecular dynamics simulation in water as explicit-solvent.	41

List of Figures

Figure number	Title	Page number
1	Classical view of modes of protein folding	2
2	Folding energy funnel	3
3	Structural changes during misfolding	3
4	UPS in ER	4
5	Development of AD in people around the world for the years 2015-2050.	5
6	Estimated lifetime risk for Alzheimer's by sex at age 45 and 65.	5
7	Aggregate remittance for AD patients 2015-2030.	6
8	Effect of AD on the brain over a period of time.	8
9	Displays X-ray diffraction pattern of amyloid fibril	8
10	Showing cryo-EM structures of (PDB: 5O3L) tau paired helical and (PDB: 5O3T) straight filaments of 3.4 Å–3.5 Å.	9
11	Amyloid fibrillogenesis	10
12	Process of Aβ aggregation	11
13	Amyloid cascade hypothesis	12
14	Process of oligomerization	12
15	A simple mechanism of MD simulation	15
16	Treatment at glance	17
17	Initial structures of $A\beta_{40}$ and $A\beta_{40}$(L34V) are displayed as a and b, respectively. The side chain of mutated residues L34V is revealed in stick style	34
18	The correlation between simulated and experimental NMR chemical shifts.	37

19	The conformations representing five most-populated microstates (m_1, m_2, m_3, m_4 and m_5) of $A\beta_{40}$ and $A\beta_{40}$(L34V).	38
20	Showing RMSD, R_g and RMSF data.	40
21	The evolution of secondary structure component as a function of simulation time (ns).	42
22	The intrapeptide side chain contacts in $A\beta_{40}$ and $A\beta_{40}$(L34V).	43
23	The solvent accessible surface area (SASA) of each residue in $A\beta_{40}$ and $A\beta_{40}$(L34V).	43

List of Abbreviations

Abbreviation	Full form
ER	Endoplasmic reticulum
UPP	Ubiquitin proteasome pathway
QC	Quality control
FAD	Familial Alzheimer's Disease
SAD	Sporadic Alzheimer's Disease
AD	Alzheimer's Disease
APP	Amyloid Precursor Protein
AICD	APP Intracellular Domain
RAGE	Receptor for Advanced Glycation end Products
LRP	Lipoprotien Receptor Related Protein
MEOX2	Mesenchyme Homeobox Gene 2
Aβ	Amyloid β
REMD	Replica Exchange Molecular Dynamics Simulations
wt	Wild Type
CHC	Central hydrophobic cluster
SEC	Size exclusion chromatography
NEP	Neutral endopeptidase
SDS	Sodium dodecylsulphate
NMR	Nuclear magnetic resonance
CD	Circular dichroism
DOPC	Dioleyl phophatidylcholine
RMSD	Root mean square deviation

MSFs	Mean square fluctuations
FELs	Free energy landscapes
MM	Molecular mechanics
FMD	Fragment molecular orbital
HCSM	Human cerebrovascular smooth muscle
ICH	Intracerebaral haemorrhages
MMP	Matrix metalloproteases
FAD	Food and drug administration
MD	Molecular dynamics
APC	Activated protein C
BBB	Blood brain barrier
RMSF	Root Mean Square Fluctuation
SASA	Solvent Accessible Surface Area

Chapter 1

Introduction

1.1Protein folding

The course of protein folding is a highly complex procedure by which a recently synthesized unfolded peptide folds into its native three-dimensional structure. Different models are proposed to explain the protein folding process which is divided into classical view and new view. Classical view which comprises of the folding pathways (Figure 1)[1] is as follows:

- **Framework model**: This model is a sequential protein folding procedure also known as hierarchy model. It proposes that the protein folding starts with the development of secondary structure elements later interacting with one another to give rise to more superior folding intermediate. The folding procedure terminates with the explicit packing of side chains. Each step forward in the process of folding is a stabilizing procedure for the previously formed elements suggestive of the presence of several folding intermediates.

- **Diffusion collision model**: The framework model is supposed to be the limiting case of diffusion collision model. The main postulate of this model suggests that the protein is formed by number of unstable quasi-particles known as micro-domains attaining stability by diffusion, collision and coalesce. Conformation generated per step brings it closer to the formation of native structure whose stability is governed by short range forces such as Van der Waals repulsion and hydrophobic interaction**.**

- **Hydrophobic collapse model**: This hypothesis is based on the condition that the native protein has its interior comprising of non-polar amino acids known as the hydrophobic core. The stabilization is brought about by the isolation of the hydrophobic amino acids from the neighbouring water molecules. The hypothesis suggests that the hydrophobic collapse is a primary event in the folding process followed by secondary and then tertiary structure and so on.

- **Nucleation condensation model**: This hypothesis proposes that the process of protein folding is identical to the process of crystallization with nucleus formation being the limiting step followed by elevated propagation of structures. This hypothesis states that there is formation of weak nucleus which is further stabilized by long range forces. The formation of nucleus is

initiated by the transition state implying minimal intermediate generation in support with Levinthal paradox. Higher proteins are thought to be the result of nucleation of modules.

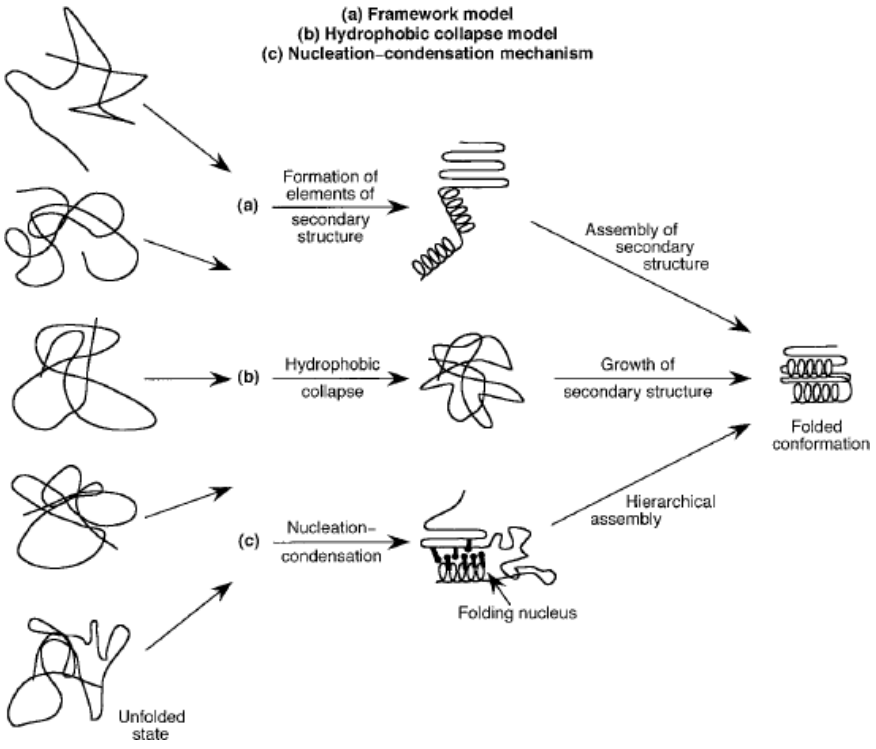

Figure 1: Classical view of modes of protein folding.

Protein folding funnel or the energy landscape: It was proposed by Joseph Bryngelson and Jose N.Onuchic (in Bryngelson et al 1995 and Onuchic et al in 1997 respectively)[2] (Figure 2). This energy landscape is known as energy funnel as the free energy is elevated for larger number of conformations and is lesser for lesser number of conformations. It states that protein folding does not take place by a single pathway but occurs by number of routes down the folding funnel. The uppermost energy level is in association with disordered state of the proteins and as the protein folds into an organized and finally to its native conformation the association is with lower energy levels corresponding to higher stability. The energy minima correspond to the native structure comprising of properly packed α and β helices.

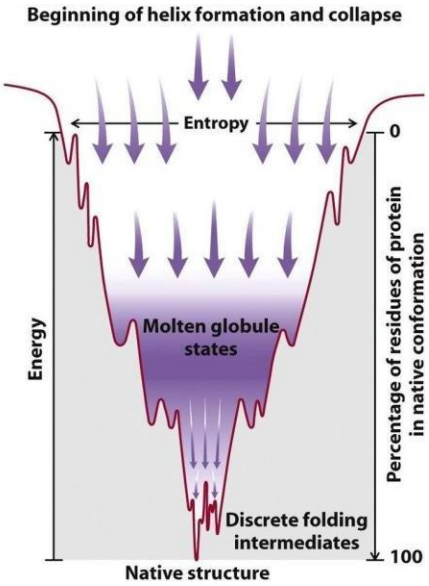

Figure 2: Folding energy funnel.

1.2 Protein misfolding

A protein is considered as functionally active when it has attained its 3D native conformation through a complicated folding pathway assisted by molecular chaperones preventing the development of a misfolded or aggregated conformation. Proteins unable to achieve the 3D native conformation as a result of mutation or due to simple error in the folding course, are known as misfolded protein characterized by excessive β sheet formation (Figure 3).[3] In Figure 3 panel A depicts native conformation with secondary α helical conformation, panel B conversion of α helix to β pleated sheet due to misfolding and panel C depicts the ultimate misfolded peptide consisting chiefly β sheet conformation.

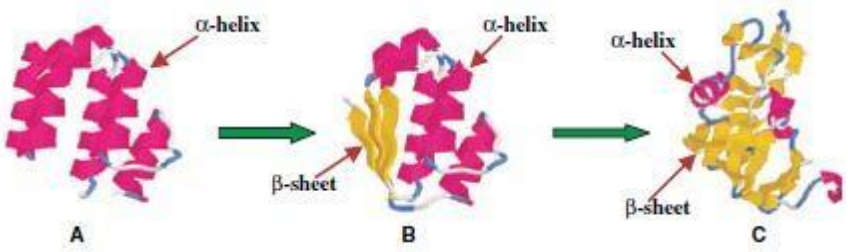

Figure 3: Structural changes during misfolding.

These misfolded proteins and are then subjected to a degradation pathway.[4] This is stated as protein 'quality control' (QC) comprising of two elements: ubiquitin proteasome system (UPS, Figure 4) and molecular chaperones. One of the most important features of QC is the ubiquitin

proteasome pathway (UPP), any disturbance or impairment inculcated by the gathering of misfolded peptides in the endoplasmic reticulum (ER) or due to the loss of enzymatic function in the ubiquitin deconjugation and conjugation pathway, leads to distorted UPS function, which affects the amassing of peptide aggregates in the cell. The generation of aggregates and oligomers occur in the cell as a result of elevated concentration of misfolded peptide. Aggregated peptides frequently lead to the generation of an amyloid-like organization causing different forms of degenerative disorders such as Alzheimer and eventually cell death.

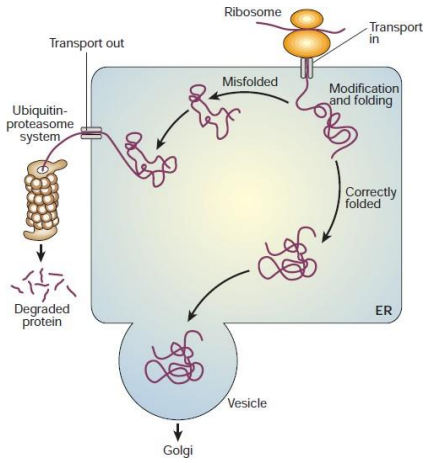

Figure 4: UPS in ER

1.3 Origin and prevalence of Alzheimer disease (AD)

Alzheimer's illness is the most well-known type of dementia representing 60-80 % of the cases. It was first perceived by Alois Alzheimer as an unconventional serious ailment of cerebral cortex in 1906, in a 50 year's old woman named Auguste Deter. The symptoms involved memory loss, abnormal behaviour and shrinkage of patient's brain, ultimately leading to death. This chronic disease is prevalent among 10 % of aged people, mainly diagnosed in people with ages over 65 making AD a noticeable social medical problem with the ascent of maturing inhabitants in the coming decades.

Everywhere throughout the world there are around 47 million individuals influenced with AD and it is evaluated to achieve 74.7 million by 2030 (Figure 5). The risks for both sexes are slightly higher at the age of 65 (Figure 6). A number of biological and social causes support the fact that more women than men have Alzheimer's. The estimation of Neugroschl and Sano (Neugroschl & Sano, 2010)[5] states that there would be a decrease of 2 million in AD cases over a period of 50 years if it's onset could be delayed by two years resulting in a decreased need

for nursing care and efficiency of caregivers. All in all AD isn't precisely a maturing related ailment. In general, it is categorized in two sorts. One is the hereditarily transmissible AD, known as the early outset familial Alzheimer's disease (FAD), which is an uncommon form accounting for 25% of all AD cases, occurring in the age group of 50-65. Another form is the sporadic Alzheimer's disease (SAD), also referred as late onset AD due to its occurrence after the age of 65. This type contains the larger part of AD cases and is additionally clearly influenced by hereditary contributions other than natural components.

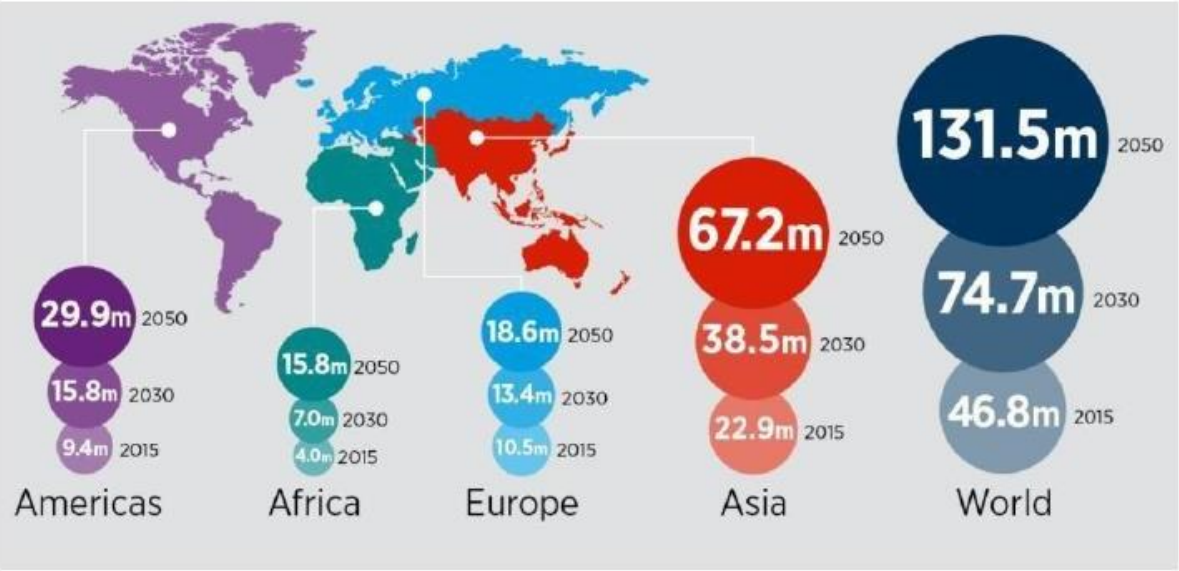

Figure 5: Development of AD in the people around the world for the years 2015-2050.

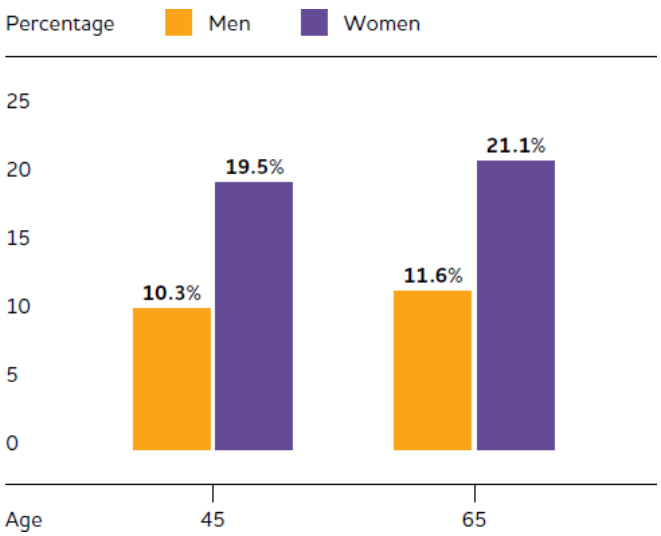

Figure 6: Estimated lifetime risk for Alzheimer's by sex at age 45 and 65.

This discrepancy arises due to the fact that the mortality rate of women is higher on average in comparison to men; also, more established age is the most serious hazard factor for AD. Estimated lifetime risk (the likelihood of advancement of a condition at a specific age amid his or her outstanding life expectancy) for Alzheimer's dementia is approximately one in five (20 %) for women and one in 10 (10 %) for men at the age of 45. Aggregate remittance for AD patients are projected to elevate from $818 billion to $2 trillion by 2030 (in dollars), indicating a climb in the costs as well as cases for AD as the population ages (Figure 7).

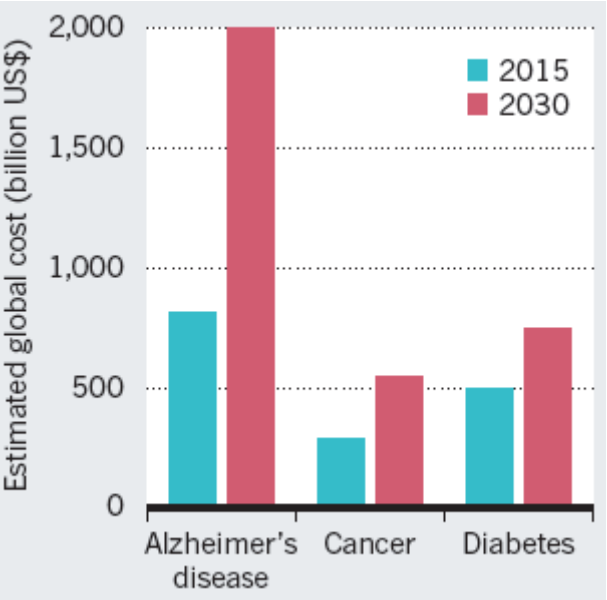

Figure 7: Aggregate remittance for AD patients 2015-2030.

1.4 Alzheimer's symptomatology

AD thrives steadily in three stages: early, middle and late. The symptoms of AD aggravate over time (Figure 8). A person suffering from Alzheimer's on an average can survive for 4-8 years after diagnosis, but depending on other factors the survival can also last up to 20 years. Alteration in the brain allied with AD arises years before any signs of the disease. This phase is assigned as preclinical AD. Stages may lap over, making it difficult to assign the patient a specific stage.

Early stage Alzheimer's: This chronic disease eventually leads to language and learning impairment, however it doesn't affect entire memory capacity similarly. Recollections of the individual's life (roundabout memory), realities learned (semantic memory), and understood memory (the memory of the body on the best way to get things done, for example, how to eat

and drink) are influenced to a lesser degree than new certainties or recollections. Common difficulties include:

a) Problems remembering the correct word.
b) Trouble remembering names when acquainted with new individuals.
c) Challenges performing undertakings, for example, composing, dressing, certain development coordination in social or work settings. Overlooking issue that was simply perused.
d) Misplacing a valuable object.
e) Planning difficulties maybe present.

Middle stage Alzheimer's: In this stage older memories which were previously intact fade away. Deportment and neuropsychiatric changes become more evident. Speech difficulties become prevalent, reading and writing capabilities are also gradually lost. Approximately 30% of people develop delusional symptoms and illusionary manifestations. The memory problems worsen enough to make the affected people forget about their relatives. At this point, symptoms will be noticeable to others and may include:

a) Often forgetting events and personal history.
b) Feeling drained or unaware, chiefly in socially or mentally demanding situations.
c) Inability to remember one's own locality or telephone number.
d) Perplexed regarding the place where they are or what day it is.
e) Difficulty managing bladder and bowels in some individuals.
f) Changes in sleep paradigm, such as resting amid the day and getting agitated during the evening.
g) An elevated fear of wandering and becoming astray.
h) Character and deportment changes, including doubt and misconception or uncontrollable stressful behaviour like hand wringing or tissue mangling.

Late stage Alzheimer's: The final phase is marked by the reduction of intellect and complete loss of speech. Extreme passivity and enervation becomes the part of patient's personality. Muscle mass and mobility decreases to an extent where the patient becomes bedridden. This phase may include:

a) Require all time assistance with daily chores and personal care.
b) Complete cognitive impairment and loss of awareness of self and surrounding.
c) Loss in the ability to walk, sit and swallow.
d) Loss of intellect

e) Vulnerable to infections.

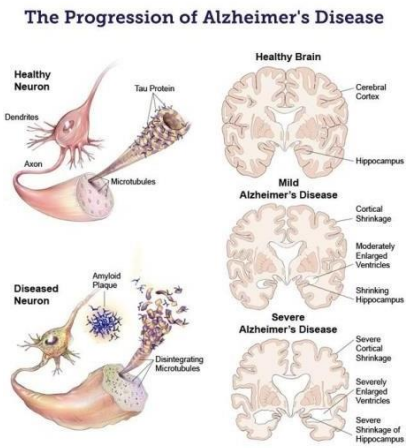

Figure 8: Effect of AD on the brain over a period of time.

1.5 Genesis of Alzheimer

Traditionally amyloid-β (Aβ) peptides are considered to be central cause of AD. These tend to form amyloid fibrils which accumulate as senile plaques known to be extracellular amyloid accumulations in the brains grey matter and generation of neurofibrillary tangles considered as insoluble twisted fibres found inside neurons. Amyloid fibrils are homopolymrers of protein stabilized by β strands comprising of intermolecular hydrogen bonding. These strands are arranged orthogonally to the axis of the fibril resulting in a highly strengthened cross β construction (Figure 9).

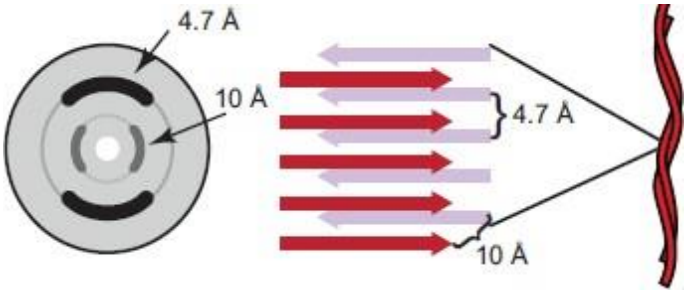

Figure 9: Displays the X-ray diffraction pattern of amyloid fibril.[4]

In the above figure chief reflections are displayed at 4.7 Å and 10 Å approximately evident of hydrogen bonding separations between side chain and β strands along with side-chain arrangement in case of β-sheets respectively.[6] The figure is also indicative of cross-β conformation comprising of β-strands arranged perpendicular with respect to the fibril axis.

The neurofibrillary tangles mentioned earlier comprise of a protein called tau which is normally a part of the microtubule a structure which helps with the transport of nutrients among different parts of the nerve cells. However in AD the tau protein acts abnormally collapsing the microtubule structure (Figure 10).

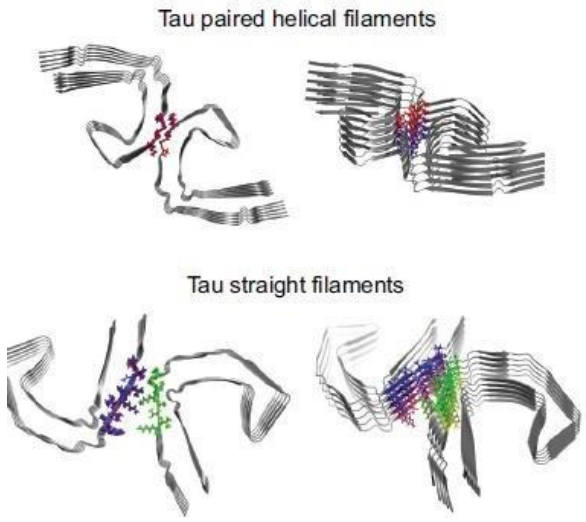

Figure 10: Showing cryo-EM structures of (PDB: 5O3L) tau paired helical and (PDB: 5O3T) straight filaments of 3.4 Å–3.5 Å.[7]

Amyloid fibrilogensis can be explained on the basis of a sigmoidal curve comprising of three stages (Figure 11):[8]

1. Lag phase: marked by the conversion of monomers to nuclei and transition of folded native state to oligomeric with β sheet conformation.
2. Exponential phase: also known as the growth phase is composed of multistep leading to arrangement of soluble species into preformed β sheet conformation *i.e*. protofibrils.
3. Saturation phase: marked by complete formation of fibrils which associate with one another resulting in mature fibrils.

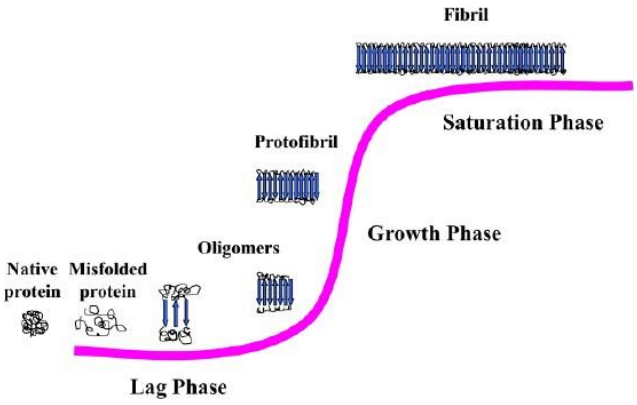

Figure 11: Amyloid fibrillogenesis.

APP (Amyloid Precursor Protein) is consecutively severed by two enzyme activities β and γsecretase forming Aβ. Firstly APP is cleaved by β-secretase to discharge an amino terminal fragment called secreted APP beta (sAPPβ). On the other hand the carboxyl terminal fragment formed by β-secretase of 99 amino acids (CTF99, which begins with the terminal N having Aspartic acid residue of Aβ) is rapidly severed by the enzyme γ-secretase to produce Amyloid β. Cleavage by γ-secretase is however inaccurate, leading to C-terminal heterogeneity of consequential peptide population. Therefore numerous dissimilar Aβ species persist. The ones ending at site 40 (Aβ40) are the most profuse (~80-90%) after which exist the 42(Aβ42, ~5-10%). Besides γ and β-secretase there is another enzyme participating in APP cleavage known as the α-secretase. β-secretase acts upon ~10% of the total APP and the residual APP i.e. 90%, is acted upon by α-secretase resulting in sAPPα and CTFα. The cleavage by α-secretase is non amyloidogenic however the cleavage by β and γ-secretase leads to amyloidogenic pathway.

APP processing incorporates two pathways (Figure 12):[9]

1. **Non-amyloidogenic pathway**: This process begins with the cleavage of APP by α-secretase with formation of soluble APPα (sAPPα) as well as C-terminal fragment α abbreviated as CTFα. The previous is followed by hydrolysis of CTFα by γ-secretase to form APP intracellular domain (AICD).
2. **Amyloidogenic pathway**: Cleaving of APP by β secretase brings about generation of N-terminal soluble amyloid precursor protein β abbreviated as (sAPPβ) along with C-terminal fragment β (CTFβ) followed by hydrolysis of CTFβ by γ-secretase yielding Aβ and AICD. PSEN mutation may result in elevated γ secretase activity resulting in plaque formation.

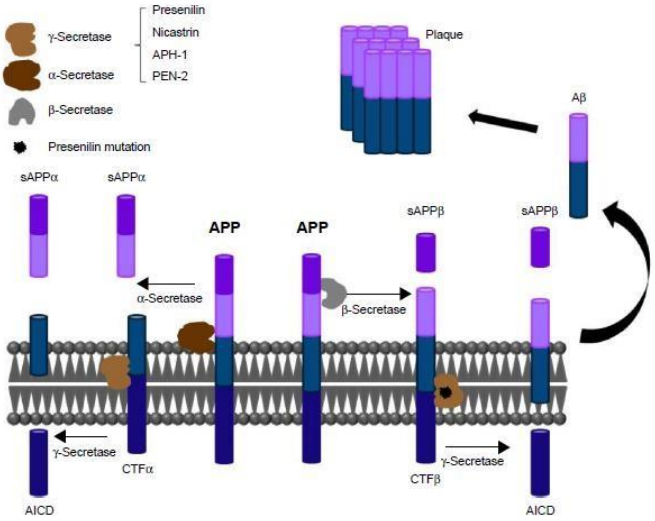

Figure 12: Process of Aβ aggregation.

The recognition Aβ of as the major component in amyloid plaques was first spotted in the mid 1980's , followed by Hardy and Higgins proposal of amyloid cascade hypothesis in their highly cited review.[10] Since 1992, this hypothesis (Figure 13) has played a major part in clarifying the etiology and pathogenesis of AD. It recommends that amyloid-β is a causative agent leading to Alzheimer's disease, the initial step being its deposition followed by other phenomenon such as formation of neurofibrillatory tangles, tau phosphorylation, vascular damage, neuronal death, dementia, and finally death.

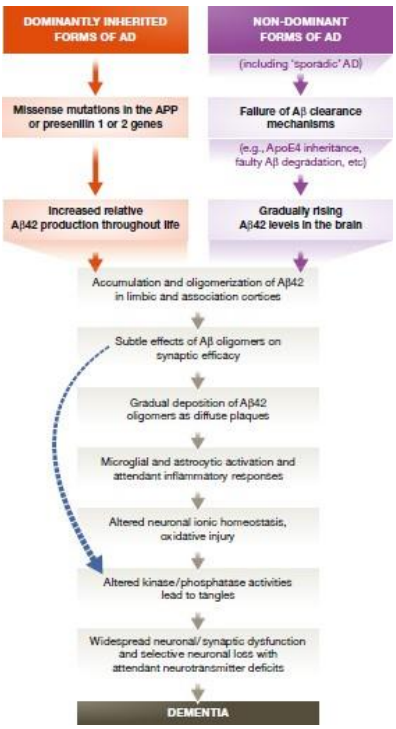

Figure 13: Amyloid cascade theory.

The bended blue arrow shows that Aβ oligomers may specifically harm the neurotransmitters and neurites of neurons alongside enactment of microglia. Several emendations brought about in amyloid cascade hypothesis have been agreed to by the research community without compromising the basic assumption of amyloid-β being the causative agent of AD. Firstly, oligomers are thought as the most neurotoxic amyloid species rather than amyloid fibrils or amyloid plaques leading to emergence of new theory referred as "oligomer cascade hypothesis" (Figure 14).

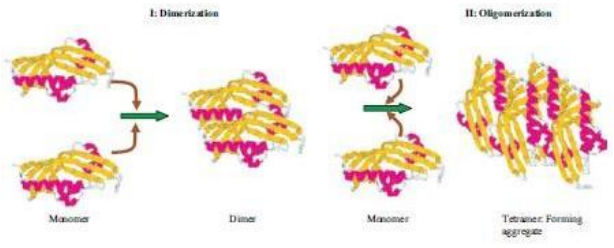

Figure 14: Process of oligomerization.[3]

Secondly, in SAD, the AD symptoms are related with the generation of more pathogenic Aβ42 [opposed to more stable Aβ40,] resulting by the incorrect cleaving of APP rather than the overproduction of amyloid-β. Traditionally, the presence of amyloid plaques in the brain, which showed apple green birefringence when stained with Congo red, was the conclusive post mortem diagnosis for AD. These plaques were considered to be the predominant cause of AD. However, past 10 years of research has stated that amyloid plaques are just associations not the causative agent of AD. Post-mortem reports of many people have displayed cerebral amyloid plaques without ever showing symptoms of Alzheimer's. The basic concept of formation of amyloid plaques is to act like "prisons" to neutralize toxic oligomers. Once the "prisons" are occupied, there are too many oligomers for the "guards" (neuroclearance mechanisms) to handle leading the oligomers to devastate the brain. Basically any Attempts to avert amyloid plaques would release the "evil ones" causing more damage proposed by Selkoe and hardy.[11] Amyloid-β aggregation can lead to number of different oligomeric structures with varying levels of toxicities. Amyloid-β when incorporated into lipid membranes has been shown to produce channel-like tetrameric and hexameric structures which appear to be most stable in lipid membranes. Amorphous amyloid does not exhibit neurotoxicity on the contrary compact amyloid deposits possess higher neurotoxicity. Stable oligomers are highly neurotoxic which can be concluded from the fact that they have the capability to induce neuronal apoptosis fifty times more than amyloid fibrils consisting of wild-type Aβ42. In comparison to monomers, trimers and tetramers have higher toxicity [3 and 13 times respectively].[12] Structural order of toxicity: is described as tetramers > trimers > dimers > fibrils > monomers.[12] In comparison to the size and structure exposed hydrophobic parts in oligomers are the primary determinant of neurotoxicity.

Metals like Cu^{2+} tend to increase the neurotoxicity of Aβ. This can be very well made out from the fact, that without Cu^{2+} the toxicity of amyloid β tends to leave viability of PC12 cells to 40% whereas addition of Cu^{2+} to Aβ42 results in viability of PC12 cells of only 4%.[13]

1.6 Therapeutic pathways for AD

Novel therapeutic targets for treatment of AD are as follows:[14]

Ischemic brain: It is one of the factors resulting in increased Aβ production hence targeting it for treatment may result in decreased AD. However the inhibition of development of Dementia and vascular disorder in AD by a new group of agents for example activated protein C

abbreviated as (APC) having combined neuroprotective, anticoagulant and anti-inflammatory activities in the ischemic brain still remains a question.

The Receptor for Advanced Glycation End Products (RAGE): It in general is exhibited at small portions in brain, whereas under pathological conditions its expression gets elevated hence forming a great therapeutic target. Preventing RAGE–Aβ cooperation in the infected veins hurdles Aβ convergence over the the BBB (blood brain barrier) along with linked oxidative stress including neuron swelling. RAGE along with Aβ inhibitors are at present under examination in Alzheimer's patients for protection with efficiency.

Low density lipoprotein receptor related protein 1 (LRP) Aβ clearance has Aβ binding to LRP as its initial step leading to transvascular Aβ transfer across the BBB. Thus forming a great therapeutic target.

Mesenchyme homeobox gene 2 (MEOX2): A current report found tremendous declining of MEOX2 expression in BBB of AD patients. Decrease in MEOX2 leads to proteasomal disintegration of LRP, followed decreased Aβ clearing tendency at the BBB hence leading to Aβ build up, therefore acting as great therapeutic targets.

1.7 Importance and limitations of molecular docking and dynamics

Molecular Docking: protein ligand docking is the process which takes into consideration the calculation and ranking of the conformations arising from the interaction between a target peptide whose 3D structure is known with a given ligand.[15] Pioneered near the beginning of 1980 it remains a ground of strong research, becoming a critical tool for finding suitable drugs. Most Molecular Docking programmes available are can anticipate protein ligand conformations including a success rate ranging from 70-80 %, still it remains a field requiring high improvement even if the protein flexibility problem is tackled. The flaws in the scoring function persist to be a major limiting factor. Scoring functions generally used in docking make several simplifications and presumptions to allow a more computationally well-organized examination of ligand affinity at the expense of accuracy. Several physical factors participating in determination of conformation are completely abandoned or not fully considered in current scoring schemes. Electrostatic interactions and entropy are a few examples. Resolution of docking also comprises of other problems except for scoring. The solvent effect along with direct involvement of water molecules in protein–ligand relations, the restricted resolutions of several crystallographic targets, and protein flexibility including both inherent structural

flexibility and conformational alterations as a result of ligand binding, are some appropriate ones.

Molecular dynamics (MD): Though crystallographic studies explain the function played by flexibility of protein in ligand binding yet the labour and expense required has resulted in bending of the researchers towards the use of computational techniques like MD.[16] MD was developed in late 1970s on the basis of Newtonian physics to simulate atomic motions. A simple mechanism of MD simulation is shown in Figure 15. Though MD simulations can correctly calculate many essential molecular motions, but they are not suitable for systems comprising quantum effects, example where transition metals participate in binding. Another drawback is that the utilized force fields require additional refinement and elevated computational demands inhibit routine simulations more than a microsecond leading to an insufficient sampling of structures in several cases.

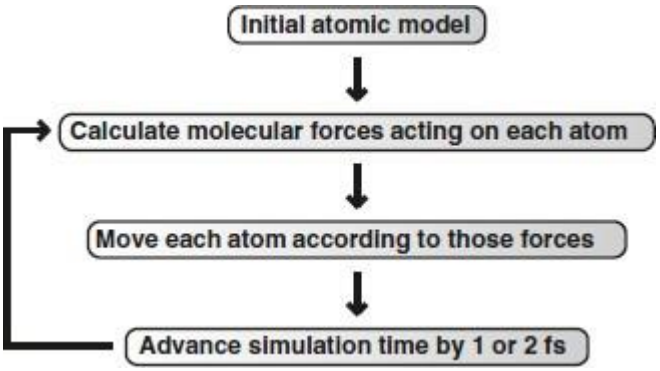

Figure 15: A simple mechanism of MD simulation

1.8 Control measures

AD is a disease of concern due to no known cure, however for the betterment of the patient following can be done:

Treatment of condition causing deterioration of health example: lung disease or anaemia.

One can promote fun activities in order to motivate the patient to pursue their normal tasks as much as possible.

a) Written reminders or photographs can be used as a memory aid that can trigger the memory of the patients making them remember the required.
b) Increased social interaction can help prevent feelings of abandonment and dejection.

c) Providing regular routine to decrease confusion.

Preventive measures: There are as such no preventive measures for AD. However epidemiologists have suggested that improved lifestyle can help to a certain extent, such as regular exercise and Mediterranean diet (vegetables, whole grain, nuts and poultry products).

1.9 Medication for AD

These cannot cure but prevent its progression (Figure 16).

Medicine for early to moderate stages: These comprise of a class of drugs called cholinesterase inhibitors. These inhibitors lead to following activities:

a) Stops the degradation of acetylcholine **(**a chemical necessary to maintain knowledge and retention power), hence helping in communication of neurons by elevating its levels.
b) Slows the aggravation of system.
c) Generally the patient is tolerant towards it however severe effects may accompany headache, puking with frequent bowel movement.

The prescribed cholinesterase inhibitors are:

a) Donepezil (Aricept) is utilized for the treatment of all phases of Alzheimer's.
b) Rivastigmine (Exelon) and Galantamine (Razadyne) is used to treat early to middle stage Alzheimer's.

Therapy for middle to late stages: Memantine (Namenda) and the amalgamation of memantine and donepezil (Namzaric) are agreed to by the food and drug administration (FAD) for treating middle to late AD. For the prevention of cognitive and rational impairment and to improve the capability to execute simple tasks Memantine is often prescribed. It can be utilized alone or with other AD treatments. A medication that incorporates both memantime and cholinesterase inhibitor is also used to obtain better results.

Memantine is used to:

- Manage the activity of glutamate (concerned with information processing, retention and retrieval)
- Boosts the intellects and the ability to perform daily chores.
- Some side effects like migraine, uncertainty and dizziness may prevail.

Generic	Brand	Approved For	Side Effects
donepezil	Aricept	All stages	Nausea, vomiting, loss of appetite and increased frequency of bowel movements.
galantamine	Razadyne	Mild to moderate	Nausea, vomiting, loss of appetite and increased frequency of bowel movements.
memantine	Namenda	Moderate to severe	Headache, constipation, confusion and dizziness.
rivastigmine	Exelon	Mild to moderate	Nausea, vomiting, loss of appetite and increased frequency of bowel movements.
memantine + donepezil	Namzaric	Moderate to severe	Nausea, vomiting, loss of appetite, increased frequency of bowel movements, headache, constipation, confusion and dizziness.

Figure 16: Treatment at glance.

1.10 Objective of the thesis

L34V is a novel mutation by the name of piedemont. It is an AβPP mutation in association with cerebral amyloid angiopathy (CAA). The pathological studies of the mutation revealed serious CAA lacking neurofibrillary tangles and pathological amyloid plaques. The *in vitro* studies have displayed restricted oligomerization or fibrillization comparable to wt $A\beta_{40}$ and in contrast with E22Q mutation. The transmission electron microscopy results state that the mutation resulted in elevation of Aβ aggregation. All the data collected by far on L34V only explains either its pathological symptoms or its potential to increase Aβ aggregation, none have discussed the molecular mechanism resulting in increased Aβ aggregation and therefore CAA. In this regard, we aim to elucidate the effect of L34V mutation on the structure, dynamics and aggregation of wt $A\beta_{40}$ peptide using molecular dynamics (MD) simulations, which, otherwise, is difficult to study using experimental techniques due to conformational heterogeneity of the wt $A\beta_{40}$ peptide. L34V becomes a centre of attraction for studying AD as:

a) It is a naturally occurring mutation.
b) Its molecular mechanism has not been studied.
c) It is an aggregation prone mutation resulting in Alzheimer, which is growing at a faster pace, taking a toll over a larger population.
d) AD has become a disease of concern due to lack of knowledge and prevention mechanism; hence needs to be reckoned.

1.11 Overview of the thesis

The thesis is segregated into chapters for a better insight into the topic:

Chapter 1: It introduces one to AD which is a result of protein misfolding. The chapter is further subdivided in order for enhanced understanding of AD. It not only takes into consideration the cause of Alzheimer but also provides various therapeutic ways to oppose it. The chapter is also accompanied with objective of the thesis to give a better viewpoint of choosing L34V as the topic for analysis.

Chapter 2: It summarises some of the work of various researchers on some common mutations leading to AD. Most of the mutations mentioned have been studied in detail for their increase in Aβ aggregation and the molecular mechanism leading to it. The studies taken into consideration are *in vivo*, *in vitro*, *in silico*, transmission electron microscopy, MD, etc. explaining for most of the mutations their pathological effects and aggregation propensity.

Chapter 3: It takes into consideration the explanation of the method utilized for analysis of the mutation taken into consideration in this thesis.

Chapter 4: It attempts to explain the reason for increased aggregation propensity due to L34V by taking into consideration the results displayed by the MD simulations.

Chapter 5: It summarises the data reported.

Chapter 2

Literature review

Das *et al.* conducted extensive atomistic REMD (replica-exchange molecular dynamics simulations) in explicit water to analogize in silicon the monomer conformational ensemble of A2V and A2T mutations with respect to the $A\beta_{42}$ wt.[17] The simulations revealed that despite the existence of the variants as collapsed coils in the solution remarkable conformational discrepancies were observed among them at small timescales. A2V displayed an intensified double-hairpin population with respect to the wt, homologous to the ones described in toxic wt $A\beta_{42}$ oligomers. The double-hairpin generation was the result of hydrophobic clustering that took place between the N-terminal and the central and C-terminus hydrophobic patches. Different to A2V the A2T variant caused the N-terminal to participate in uncommon electrostatic interactions with remote residues, for example K16 and E22, leading to a distinctive population including only the C-terminal hairpin. Combination of the results suggested that the A2V/T mutation mainly altered the β-hairpin interactions taking place between the CHC (the central hydrophobic cluster) and the C-terminal referred as NCCHC-CTR. Other than that the interactions between the N-terminal (Ntr) (residues 1–5) and the CHC, referred as NCNtr-CHC were also affected. Overall findings suggested that both the mentioned mutations in the primarily disordered N-terminus of the $A\beta_{42}$monomer can markedly alter the β-hairpin population and change the equilibrium towards alternative structures.

Giaccone *et al.* for the first time reported the pathological symptoms of a patient consisting FAD caused due to a recessive mutation.[18] Their report provided a detailed account of the neuropathological aspect of the proband affected with A673V mutation. They conducted immunohistochemical and histological tests to study the brain of the proband at the ultrastructural and optical levels. The results showed Aβ accumulation in the cerebral region of the brain including extensive tau pathology. The area of concern was the large sized configuration chiefly perivascular and showed an intimate association between the paradigm obtained by amyloid staining and the labelling elicited by immuno reagents specific for Aβ42 and Aβ40. The Aβ deposition did not affect the neostriatum however heavily affected the cerebellum and was therefore not in conformity with the pattern of participation recognized in sporadic AD. Therefore, the neuropathological image of FAD induced by A673V offer unique characteristics in comparison to SAD or FAD inherited as a governing trait. Mainly the unusual

characteristics are the morphology, conformational properties and composition of amyloid β accumulation and their topographic allotment in the brain.

Ono *et al.* examined the monomer conformational dynamics and oligomerization and found that in comparison to their wt homologues and in the respective systems of Aβ40 and Aβ42, the English (H6R) and Tottori (D7N) mutations elevated the kinetics of secondary conformational change taking place from statistical coil to α/β and finally β producing oligomers. The observation was depicted as a rise in average oligomer size measured by utilizing electron microscopy and atomic force microscopy.[19] In situ chemical cross linking was used to stabilize peptide oligomer allowing detailed study of their properties. The mutations lead to formation of oligomers that showed predominant β-strand in English mutation or α/β in Tottori mutation, different with respect to predominant statistical coil structure of wt Aβ oligomers. Analyzation of the stabilized oligomers per system displayed a constant order of size as English > Tottori > wt. The order was similar with respect to of β-strand amount in the oligomers .They completed their research by analyzing the biological activities of the substituted peptides in comparison to their wt homologues. Results displayed that H6R and D7N variants were capable of altering Aβ assembly at its initial stages, monomer folding and oligomerization, producing oligomers which acted as fibril seeds with higher potential in comparison to their wild type homologues. The overall results supported the conclusions that: 1) stabilization of the oligomers remarkably increased protein toxicity; and 2) the H6R and D7N mutations had the potential to further elevate the toxicity by affecting the kinetics of peptide aggregation and the structures of the aggregation thus formed.

Xu *et al.* using REMD simulations investigated the effect of modulation of N terminal on the thermodynamic stability, overall conformations and coordinated domain motions of amyloid β, the FAD mutations namely Taiwanese (D7H), Tottori (D7N), and English (H6R).[20] They observed each mutation elevated β-sheet tendency of both termini, predominantly the C-terminal area, however in all there is no change in the tertiary structures of these mutations. Utilizing both the MM/ GBSA52 and MM/3D-RISM techniques, they realised that these mutations inculcated instability in Aβ42 monomer due to the elevated solvation free energy, leading to formation of more toxic oligomers. Further observation lead to the conclusion that low to mild structured conformations were differently altered by mutated N terminus. They observed that the mutations might have discrepancies on the basis of effects with respect to the binding of metal ions as D7H consist an extra histidine, whereas H6R is deficient of one metal

binding histidine. On the other hand D7N could vary the susceptibility of its neighbouring histidine with respect to metal ions. To nucleate folding of Aβ, the conserved turn structure at Valine24–Lysine28 in all proteins and Aβ42 bound to Zn^{2+} was confirmed to be the general structural motif. Each mutation significantly increased the solvation free energy thus elevating the aggregation propensity of Aβ monomers.

Viet *et al.* utilized all-atom molecular dynamics simulations to understand the influence of the Tottori mutation (D7N) on the conformations of Aβ40 and Aβ42 considering the random coil monomeric conformation and the fibrillar dimeric conformation.[21] 3 μs monomer simulation starting from a random coil displayed that the D7Nmutation changed the folding and the network of salt bridges in both systems. Another 4.4 μs dimer simulation beginning from the amyloid fibrillar states revealed the changes with respect to secondary structure, topology and salt bridge. As a whole the data was in support of the experimental finding of D7N mutation accelerating fibril generation of Aβ40 and Aβ42 peptides. For both alloforms, they found an enhanced rate of formation of Aβ40 fibrils by generation of the loop Asp23-Lys28 in the monomer, resulting in higher fibrillar-like states in D7N dimer in comparison to wt dimer. Contrastingly the elevated rate of formation of Aβ42 fibrils did not result by the generation of the loop Asp23-Lys28 in monomer, but could have resulted by the generation of the same loop in dimer. Their simulations for the first time provided an insight on the Aβ-D7N dimeric and monomeric conformations in explicit solvent and also showed an atomic level picture of the influence of D7N mutation on the conformational change in Aβ40 and Aβ42 peptides.

Kaden *et al.* elucidated role of K16N in AD by in vitro analysis. Size exclusion chromatography (SEC) was conducted for the three peptides Aβ40, Aβ42 and K16N respectively to see whether the mutation has any effects on initial phases of the peptide aggregation.[22] Analyzation of equimolar mixture of the peptides was also taken into consideration. The results showed that Aβ40 wt, Aβ40 K16N, mixture of Aβ40 wt and Aβ40 K16N, Aβ42 wt and Aβ42 K16N formed lower number of oligomers lacking higher aggregates. On the contrary, mixture of wt Aβ42 and Aβ42 K16N formed larger number of oligomers. Toxicity of the mutation was also tested in vitro, the results displayed Aβ42 K16N peptides to be predominantly less harmful to neuronal cells in comparison to Aβ42 wt whereas the Aβ42 mix showed an elevated amount of toxicity similar to the wt Aβ42.In general the Aβ mix was showing increased aggregation property which was justified by the conformational model of Aβ wt and K16N heterogenous tetramers based on the Aβ42 structure. The model suggested that the stabalization of β-sheet

structure was due to the formation of a hydrogen bond between the side chains of K16 and N16 residues this bond was absent in the wt peptides. The stabilized heterogenous structures accounted for the increased aggregation and toxicity of the Aβ42 mix. The Aβ42 K16N peptides are shielded with respect to clearance activity conducted by the Aβ-degrading Enzyme Neprilysin (NEP). Thus K16N examined by them comprises an amalgamation of risk factors that in combination could contribute to the blooming of early onset AD. The results illustrate that the APP K16N mutation has more than a single characteristic to make it pathogenic which can be summed up as (i) APP processing and (ii) characteristics of the mutated peptide that is aggregation, stability and toxicity.

Motowidło *et al.* have their study conducted on the membrane structures of Aβ(11-28) mutations (Italian and Flemish) in comparison to the familiar conformation of the native Aβ(12-28) fragment utilizing 2D NMR data, CD and MD methods under water-SDS micelle.[23] The fragment chosen is considered crucial for amyloid fibril formation. NMR studies displayed two definite portions of proton resonances for the fragments. Examination of the peptides marked the presence of α helical structure in the Italian mutation, different to which was the Flemish being unstructured having the chances of a bend conformation in the centre of the fragment. The conformational analysis of the peptides was studied utilizing NMR spectroscopy and circular dichroism (CD) spectropolarimetry in a membrane-mimicking (sodium dodecylsulfate, SDS). CD examination were performed in the absence as well as presence of SDS micelles, on the other hand the NMR experiments were carried out only in its presence. The fragment and water molecule interaction was examined in terms of hydration number. The observations displayed that for both heavy atoms of side chain and carbonyl oxygen the Italian fragment had a distinct first water shell in comparison to the Flemish one. The Italian fragment had Val12, His13, Phe19, Lys22, Asp23, Val24, and Lys28 side chains highly exposed to aqueous environment contrary to the Flemish variant where the side chains were are His13, His14, Phe20, Glu22, Asp23, Val24, and Lys28. The highest hydration number displayed by Lys22 residue of the Italian Aβ segment suggested that it is highly exposed to water molecules.

Jang *et al.* performed 100 ns explicit MD simulations of Osaka mutation and Aβ42 wt peptides in a DOPC (dioleyl-phophatidylcholine) bilayer.[24] The monomer mutant conformation was obtained by the deletion of Glu22 in Aβ1–42 peptide. Utilizing MD simulations, two ΔE22 barrels having monomer conformation in the form of U obtained from NMR-based wild type Aβ fibrils were examined in explicit lipid Surroundings. The results displayed that the ΔE22

barrels attained the lipid-relaxed β-barrel like channel. Even though the ΔE22 barrels lack the cationic binding location in generally provided by the Glu22 side-chains, a new cation binding location is obtained by the pores of the mutant by virtue of Glu11. The mutant proposed that toxic wt Aβ1–42 would predominantly accept a decreased C-terminus turn identical to the one for for Aβ17–42, and elucidated the reason of solid state NMR data for Aβ1–40 displaying a more C-terminus turn conformation. The examined ΔE22 barrels preferential conformation also accounts an explanation for the decreased neurotoxicity in neurons of a rat in comparison to the wt Aβ1–42. Concluding that the Molecular Dynamic simulations provided a membrane bound conformation of the ΔE22mutant barrel stating that the multimeric β-barrel-like channel could be identical to the wt Aβ1–42 barrel. With a pattern of β-strandturn-β-strand the U-shaped peptide supported the Osaka mutation barrel, stating the general Aβ pattern of aggregation. The higher hydrophobicity leading to faster oligomerization and fibril formation is due to the loss of charge. They observed that elevated formation of oligomers due to mutation could result in toxic channel generation finally leading to oligomers incorporation into cell membrane in Familial Alzheimer disease.

Bossis and Palese reported the initial conformational changes of the Aβ-42 peptide by an all-atom molecular dynamic in aqueous environment.[25] They studied the conformational transitions in the Aβ42 in distinct conditions that is in water with decreased and increased ionic concentrations respectively. The RMSD data revealed the structural journey of the peptide moving steadily towards steady conformation ensemble with a general RMSD of not more than 5 Å from the initial structure. The data stated no change in the N-terminal helix however the change was observed in the ultimate C-terminal end of the peptide (i.e. prominently a hydrophobic region) showing a prominent conformational rearrangement. Smaller segments of 3_{10}-helix appeared consisting transient residues Lys28-Gly29-Ala30 and more persistent residues Gly38-Val39-Val40 (for about 35 ns). No particular long-term interactions were observed between the Aβ-42 peptide and the sodium ions in the reduced ion concentration. With respect to Aβ42, the effect of the Dutch (E22Q) mutation in increased ionic concentration was also explored. The Dutch mutant of Aβ42 in increased ionic concentration revealed a dissimilar dynamics in comparison to the wt form. Simulations of around 2.5 ns lead the protein to show a swift structural transition having energy minima away from the initial conformation. The overall transition is rapid enough to end in less than 10 ns. TheE22Q mutant's RMSD oscillates around 9 Å as the mutant accepts a collapsed conformation as a result of its C-terminal hydrophobic part. This conformational transition was due to the loss of the hydrogen

bond which was generally seen in the other simulations of the wild type Aβ42 peptide both in increased and decreased ionic strength conditions. Clustering of hydrophobic residues is the reason for E22Q to assume a two helix collapsed structure, this study helped in gaining an understanding of the unfolding pathway of the Aβ peptide.

Blinov *et al.* aimed for the comparative study of the conformational stability and association thermodynamics of the β- sheet wt Aβ17–42 oligomers with the dissimilar protonation states of Glu22, and that of E22Q (Dutch) mutants, using all-atom MD, molecular mechanics amalgamated with solvation evaluation using statistical-mechanical, 3D molecular theory of solvation (referred to as 3D-RISM-KH) in a new MM-3D-RISM-KH method.[26] The association free energy of tiny oligomers displayed linear trend stating dimers to be more thermodynamically stable in comparison to the larger ones. The unilateral arrangement of monomers observed (in the β sheet oligomers) leads to the linear dependence of the association free energy on the size of the complex. There is a charge reduction of the wt-Aβ 17–42 Oligomers resulting from the protonation of the Glu22 which is exposed to the solvent at acidic conditions leading to lowering of the association free energy in comparison to the wt oligomers at neutral pH and the E22Q mutants. Peptide neutralization due to the E22Q mutation had a marginal affect on the association free energy and also leads to the lowering of the electrostatic interactions which are compensated by the unfavourable electrostatic solvation effects. In case of the wt oligomers in acidic phase due to absence of such compensation the electrostatic interactions accompanied with the gas-phase nonpolar energetic and the overall entropic effects contributed to the decrease in association free energy. The destabilization of the inter- and intrapeptide salt bridges between Asp23 and Lys28 resulted in the dissimilarity in the association thermodynamics among the wt-$A\beta_{42}$ oligomers at neutral pH, the Dutch mutants and the Aβ17–42 oligomers with protonated Glu22.The structural changes of the β-sheet oligomers during the MD simulations were examined using the Root Mean Square displacements (RMSDs) and Mean-Square Fluctuations (MSFs) of the backbone atoms. The RMSDs gave useful information regarding the stability of the oligomers.

Xu *et al.* performed dihedral dynamics analyses with a total of 800 ns simulation for each system.[27] The dynamics combined dPCA, PMF calculations and MSMs which were used to explain the different free energy landscapes (FELs), the microstates or macrostates and PMF of single dihedral angle, for several of Aβ42 mutations like Flemish A21G, Japanese E22Δ Arctic E22G, Dutch E22Q, Italian E22K IowaD23N, and M35 oxidation Met35OX). The

simulations of respective system resulted in displaying, that single point mutation was enough to bring about a change in the rugged FEL of Aβ42 brought about by alteration of the energy barriers around basins. The potential of each dihedral angle also proposed the alteration to varying degrees; however most minima of PMF did not shift. MSMs further unveiled that E22 mutants and D23N created mostly hub-like microstates in comparison to wt Aβ42 resulting in different alternative routes for structural transitions and elevating subsequent aggregation. Different to A21G and Met35OX where the preference is given to the transitions within the same microstate. Mapping MSM to FEL revealed that transitions between dissimilar sets of microstates were kinetically feasible but thermodynamically challenging. The trajectories generated from REMD simulations were utilized to construct the free energy surface per system utilizing dihedral principle component analysis to provide a basic idea of the influence of mutations on the energy landscapes of Aβ42. To build a MSM, conformations of each system were clustered according to ϕ and ψ dihedral angle pairs. The dissimilar effects of the mutations on the aggregation propensity could be stated as a result due to the elevation or decrease of hub-like microstates in comparison to wt Aβ42.

Nilsberth *et al.* combined the in vitro and fibrillization studies of Arctic mutation which is an APP mutation, found in the Aβ sequence at codon 693 causing AD in a Swedish family.[28] The mutation carriers displayed decreased plasma levels of both Aβ40 and Aβ42 in comparison to healthy family individuals. The Aβ42 concentration was also decreased in media by cells diseased with APPE693G. Fibrillization analysis revealed no dissimilarity in fibrillization rate however Aβ having Arctic mutation produced protofibrils at a much elevated rate and in excessive quantities wt-Aβ. The elevated protofibril generation and reduced Aβ plasma levels in the Arctic mutation may show another pathogenic pathway for Alzheimer comprising increased Aβ protofibril generation resulting in increased build-up of insoluble Aβ oligomers with patients having clinical features of early-onset AD. The *in vitro* studies revealed that the Arctic mutation had elevated tendency to generate protofibrils. The combined data by far stated that in patients having Arctic mutation, an alternative pathogenic pathway for Alzheimer operates having elevated Aβ protofibril generation as a primary event.

Okamoto *et al.* investigated stable solvated structures of wild type Aβ40 dimer and D23N (Iowa) mutation depending on their conformations, utilizing MM (classical molecular mechanics) and FMO (ab initio fragment molecular orbital) techniques, in order to display the influence of the Iowa mutation on conformation and interaction of Aβ monomers.[29] The data

elucidated that firstly the parallel conformation was more stable in comparison to antiparallel resulting from the large hydration energy for parallel structure in case of both the wild type and the D23N. Secondly the stability of the parallel conformation of wild type dimer was due to the salt-bridge between Lys28 and Asp23, electrostatic interactions between Aβ residues and the large hydration energy. Thirdly the reduced parallel conformation in case of D23N mutation was the result of loss of the salt-bridge between Lys28 and Asp23. The prediction was that the formation of salt bridge resulted in oligomerization and fibrillation of the dimmers.

Nostrand *et al.* in their study investigated wt and the mutated form of Aβ for its toxic and fibrillogenic affect on human cerebrovascular smooth muscle (HCSM) cells along with the pathogenic Aβ pattern and D23N AβPP processing. The results displayed no affect on the AβPP processing by Iowa and Dutch mutations.[30] However the Flemish mutation resulted in an elevation of 2.3 fold in Aβ secretion. The Iowa, Dutch and their double mutants lead to rapid fibril formation contrary to the Flemish mutation. The two mutations and their double mutants resulted in elevated pathological affect on HCSM, with double mutants having more potential. The results suggested that each mutation had different pathological mechanisms. The Flemish mutant is capable of increasing Aβ production whereas Iowa and Dutch mutations elevate fibril formation and pathological effect on HCSM.

Argyri *et al.* did an in vitro analysis in order to evaluate the results of the Pittsburg (L28P) mutation on the functional and conformational properties of apoE4.[31] The results displayed that the L28P substitution in apoE4 leads to the introduction of a proline residue in an increasingly helical segment of the peptide resulting in decreased favourability for α helices due to its the structural rigidity. Overall findings of the team stated that the Pittsburg mutation lead to a prominent structural and conformational restriction in apoE4 and leading to Aβ42 accumulation. They proposed that this substitution was not restricted to local region but instead was transmitted into the folding integrity of N terminal of apoE4 stating that the substitution altered the folding pathways of the peptide resulting in alteration of the kinetic and final products. The results displayed that the mutation leads to the promoted accumulation of Aβ42 intracellularly finally resulting in AD.

Subramanian *et al.* analysed the results of the I32E and V36K mutations which were non fibrillogenic and dissimilar with respect to endogenous Aβ.[32] The results stated that these substitutions resulted in the destruction of intermolecular interactions in the β2 strand and also introduced an extra possibility of interactions between the salt bridge and side chains at the i-

i+4 sites. These mutations introduced helical conformation and elevated the hydrophilicity, leaving the homologue with decreased toxicity and amyloidogenic potential.

Liang *et al.* examined the role of L17A/F19A mutations on the conformations of wt and E22G Aβ40 by utilizing Nuclear Magnetic Resonance(NMR) along with CD spectroscopies.[33] Labelled isotopes that were Aβ40, Aβ40(L17A/F19A), Aβ40 (E22G), and Aβ40(L17A/F19A/E22G) were prepared for NMR characterization. The NMR study revealed the structural difference between the mutated and wt Aβ40 stating that there was a noteworthy chemical shift represented by amide proton and nitrogen cross peaks of the L17A/F19A mutations with respect to wild-type Aβ40. On the other hand CD spectra showed two bands with minima having negative ellipticities at 206-220 nm. The spectral pattern indicated presence of α helices in the peptides. Increased negativity for Aβ40(L17A/F19A) substitution in comparison to wt was indicative of higher α-helicity in the mutated form rather than wt which was the same case for Aβ40(L17A/F19A/E22G) with respect to Aβ40(E22G). These results elucidated the reason for L17A/F19A mutation to elevate the conformational stability of the two Aβ40 proteins.

Motowidio *et al.* demonstrated that the dissimilarity between the monomers i.e. the wt cystatin C and its L68Q mutant was responsible for elevated propensity of the L68Q amyloidogenesis.[34] The simulations of wt cystatin C and L68Q monomers were examined within ns time scale using MD simulations at 308 K performed utilizing AMBER7.0 program. The results stated that the β1-α-β2 segment of L68Q variant was more dynamic in comparison to the same segment of the wt protein. The elevated flexibility of the segment explained the higher propensity of the L68Q cystatin C variant for formation of dimer. Additionally, it was displayed that the α helix of L68Q variant contrary to the wild type cystatin C is highly away with respect to β sheet interface. Another discovery was that L68Q monomer had its surface more exposed with respect to wt in the solvent. In denaturating atmosphere there were one or two salt bridges in the wild type cystatin C to act as a "molecular pin" leading to its higher stability than the L68Q mutant. The exceptionally elevated discrepancy of the non-bonded interaction between the α and β interfaces of the two monomers leads to the destabilization of the L68Q mutation and acts as a driving force for the process of dimerization.

Shimojo *et al.* reported the enzymatic investigation of γ-secretase derived from I213T substitution PS1-expressing, PS1/PS2-lacking cells and also from the brain of mice having I213T mutation.[35] Kinetics examination displayed that the Familial AD mutation decreased a

new Aβ generation, stating that substitution impairs whole of the catalytic rate of γ-secretase. Analysis per Aβ species displayed that the Familial AD mutation in particular reduced Aβ40 levels more dramatically than Aβ42 levels, resulting in an elevated Aβ42/Aβ40 ratio. In contrast, the Familial AD substitution elevated the formation of longer Aβ species comprising of Aβ43, Aβ45, and > Aβ46. The results were established by examination of γ-secretase taken from I213T knock-in mouse brain, having reduction of anew Aβ generation allele dose-dependent. Their results evidently state that the method underlying the elevated Aβ42/Aβ40 ratio examined in cases of Familial AD mutations is in relation with differential inhibition of γ site cleavage reactions comprising reaction generating Aβ40 was subject to increased inhibition than that generating Aβ42.

Korn *et al.* investigated a series of mutations of L34 such as leucine, valine, and isoleucine to state that these replacements showed minute alterations in structure of Aβ40 rising the question as to how these alterations test the dynamics, fibrillation kinetics, conformation, and toxicity of the Aβ40 aggregates.[36] Analyzation consists of kinetic studies utilizing thioflavin T and electron microscopy, for the study of fibril morphology X-ray diffraction was used, NMR experiments for local conformation and molecular dynamics analysis also came in handy. The results showed that all the mutations led to decrease in the toxicity as the hydrophobic contact between F19 and L34 is disrupted which is crucial for oligomer stability and increased toxicity. As the oligomer was the main reason of cell toxicity the results displayed shorter lag time for the mutants and accelerated fibrillation time in which oligomer concentration is decreased. These investigations not only covered a wide range of different mechanisms but were also increasingly sensitive to minute modulations of the crucial contact. There work also showed that the contact is not only governed by general hydrophobic interactions but is also dependent on stereospecific mechanisms.

Obici *et al*. reported a novel Aβ mutation (L34V) *i.e*. the Piedemont mutation in relatives with autosomal dominant, persistent intracerebral haemorrhages.[37] They performed *in vivo* analysis and disclosed that the patient had severe CAA and fatal ICH lacking neurofibrillary tangles or parenchymal amyloid plaques. Specific immune staining of amyloid with anti–Aβantibodies stated the presence of Aβ40 and Aβ42 species. 4G8 antibody established the absence of amyloid plaques and amorphous Aβ aggregates. The effect is said to be majorly caused due the abnormal hydrophobic contribution which favours the aggregation of valine in position 34 more than leucine in β- sheet structure.

Fossati *et al.* performed in vitro analysis for structural investigation of the aggregation and fibrillization properties of a novel L34V mutant relative to E22Q and the wild type Aβ40 and Aβ42.The restricted degree of oligomerization or fibrillization examined in L34V was comparable with wild type Aβ40 and contrasted with E22Q.[38] The data indicated that wild type Aβ40 which is generally unstructured in solvent comprises certain regions of conformational order. The protease resistant fragment consisting residues 21–30 assumed a bend configuration in solution serving as a folding nucleation site. The stabilization of the turn was a result of hydrophobic interactions between Valine24 and Lysine28 in addition with long range interactions occurring between Lysine28 and either Glutamic acid 22 or Aspartic acid 23. Computational studies indicated that the Dutch mutation destabilized the turn and resulted in increased oligomerization tendency persistent with their data. Contrasting to the Dutch mutation L34V had an unchanged Glutamic acid at position 22 which allowed the generation of the salt bridge resulting in increased stabilization of the conformation with high resistance to aggregation which was in agreement with their experimental results.

Guillamon *et al.* investigated the Matrix metalloproteases of brain-endothelial cell response when challenged with wild type and Aβ substituent examining their effect on Aβ fibrillization and degradation homeostasis.[39] The *in* vitro examination utilizing recombinant MMP-2 supported the protease activity and indicated that EC-released MMP-2 contributed to the production of Aβ-(1–16). However the previously mentioned Aβ degradation segment is not only the major MMP-2 produced cleavage product of Aβ40 and Aβ42 polypeptides but it is also an element of human CSF. Actually cerebrospinal fluid A-(1–16) possibly indicates a brain clearance pathway as the protein displays deprived aggregation tendency and lacks neurotoxicity.

Hatami *et al.* using transmission electron microscopy found that most of the Familial AD mutations elevated the tendency of aggregation of Aβ.[40] The Familial Alzheimer disease variants also result in the formation of substituent amyloid conformations illustrated by monoclonal antibodies and resulted in generation of discrete aggregate morphologies as per the transmission electron microscopy. Besides this many mutant proteins showed excessive decrease within thioflavin T fluorescence, irrespective of generating profuse fibrils stating that thioflavin T is a probe of structural polymorphisms rather than a dependable indicator of fibrillization. Combined results displayed that Familial AD mutations that fall in the Aβ sequence resulted in drastic modifications in oligomerization kinetics and control the ability of

Aβ to form morphologically and immunologically diverse amyloid structures. The overall data highlights that on one hand MMP-2 secretion results in an *in situ* Aβ degeneration along with detained apoptosis induction and on the other hand the increased MMP-2 secretion mainly in association with Aβ substitution related with phenotypes of ICH combined with the identified capacity of MMPs to disrupt extracellular matrices, basement membrane elements, and junction proteins proposed that CAA-Aβ might unwillingly compromise blood brain barrier integrity and result in precipitation of a hemorrhagic phenotype.

Panda *et al.* analyzed the mutations (A22G, E22G, E22K, E22Q, D23N and L34V) to understand their effect on aggregation.[41] The mutations to be analyzed were brought about by Swiss PDB viewer and were subjected to MD using NAMD to check the variation in stability and structure of the peptide. Their deviations were characterized using RMSD and plots were generated utilizing chimera. The variations lead to the generation of β fibril which were predicted utilizing PASTA2.0 and stability of the mutations were examined using PolyPhen 2.0. The results obtained stated that the substitutions at particular positions resulted in instability. The aggregation profile plots formed by PASTA 2.0 suggested that the probability of generation of β sheets in Aβ42 clearly indicated that the mutational changes have an effect on the helix conformation and consequently lead to generation of β sheets in suitable time intervals that were achieved by using RMSD deviation plots formed and simulation approach. L34V was measured as the common substitution which displayed a significant disparity as compared to wt Aβ42 and the proline mutation at E22P and L34P slowed down the aggregation of the protein.

Table 1: Summary of the mutations

Name of mutation	**Mutated residue**	**Pathological effect**	**Effect on Aβ aggregation**	**References**
A2V	A2V	Presence of perivascular aggregates with rigorous cerebellar and cerebral pathology no effect on neostriatum	Elevated production and increased aggregation	17, 18
English	H6R	Intensified cellular toxicity by oligomers, extra systematic seeding ability	Unaltered total Aβ levels, enhanced fibril generation with no elevation in protofibril levels, increased elongation period without affecting nucleation	19, 20
Tottori	D7N	Increased cellular toxicity by oligomers, extra systematic seeding ability	Unaltered total Aβ levels, enhanced fibril generation with no elevation in protofibril levels, increased elongation period without affecting nucleation	19, 20, 21
K16N	K16N	Generates proteolysis-resistant aggregates, K16NAβ42 prevents fibrillation of wt Aβ42	Elevated production	22
Flemish	A21G	Deposits in smooth muscle cells of brain causing serious CAA, Lacks toxicity towards vascular smooth muscle cells in vitro. Proteolysis-resistant aggregates	Elevated secreted Aβ, steady fibrillation	23, 27, 30

Osaka	E22Δ	Formation of fibrils, intensified ThT fluorescence of fibrils, change of toxicity profiles of Aβ42 and Aβ40	Reduction of secreted Aβ in favor of intracellular aggregate generation, enhanced aggregation	24
Dutch	E22Q	Generates vascular amyloid, reduces aggregation in brain parenchyma. Proteolysis resistant aggregates and vascular smooth muscle cells.	Elevated aggregation, unaltered APP processing	25, 26, 27, 30
Italian	E22K	CAA along with absence of neurofibrils, proteolysis-resistant aggregates	Increased aggregation of stable oligomers	23, 27
Arctic	E22G	CAA along with presence of proteolysis-resistant aggregates, oligomers are smaller but highly toxic with respect to wt Aβ	Increased protofibril generation, decreased plasma levels of Aβ	27, 28, 33
Pittsburg	L28P	Resulted in autosomal dominant AD with extensive amyloid deposits	Increased Aβ production	31
I32E	I32E	Non fibrillogenic, reduces amyloidogenic potential	Resists Aβ aggregation and fibril formation	32
V36K	V36K	Non fibrillogenic, reduces amyloidogenic potential	Resists Aβ aggregation and fibril formation	32

Taiwanese	D7H	Increased cellular toxicity by oligomers, extra systematic seeding ability	Unaltered total Aβ levels, enhanced fibril generation with no elevation in protofibril levels, increased elongation period without affecting nucleation	20
Iowa	D23N	CAA along with reduction in occurrence of stroke, consists speaking problems.	Elevated rate of fibril generation, unaltered APP processing	27, 29, 30
L17A/F19A	L17A/F19A	Obstruct the formation of amyloid fibril, decrease cytotoxicity.	Increase α helicity in turn resisting Aβ aggregation and fibril formation	33
L68Q	L68Q	Amyloidogenic forming amyloid deposits instinctively in the brain arteries. This process results in brain haemorrhages and ultimately death	Enhanced Aβ aggregation	34
I213T	I213T	Increases Aβ42/Aβ40 ratio resulting in acceleration of parenchymal Aβ deposition.	Enhanced Aβ aggregation	35
Piedmont	L34V	Results in movement disorders, absence of plaques and neurofibrillar pathology, presence of toxic.	Hypothesized to accelerate Aβ aggregation	36, 37, 38, 39, 40, 41

Chapter 3

Computational details

3.1 Preparation of systems for simulation

The coordinates intended for the wt Aβ40 having an amino acid sequence of DAEFRHDSGYEVHHQKLVFFAEDVG25SNKG29AIIG33LMVG37GVV was extracted from the NMR structures established in aqueous SDS micelles at the pH of 5.1 (PDB ID: 1BA4).[42] The PDB (1BA4) taken in this project has already been a part of several researches taking into consideration the investigation of the conformation and dynamics of Aβ40 monomer and its response to inhibitors. PyMol was utilized to mutate the amino acid residues in $A\beta_{40}$ utilizing mutagenesis tool.[43] The initial structures of $A\beta_{40}$ and $A\beta_{40}$(L34V) are displayed in Figure 17 in a and b respectively. In order to conduct the simulations of Aβ40 or its mutated form *i.e.* L34V the peptide was placed in an octahedron box of appropriate size. The octahedron box was then solvated with water molecules which were treated explicitly utilizing the three point (TIP3P) model. The solvated system was then subjected to energy minimization. The neutralization of the system was carried out by addition of Na^+ ions as per requirement to the octahedron box.

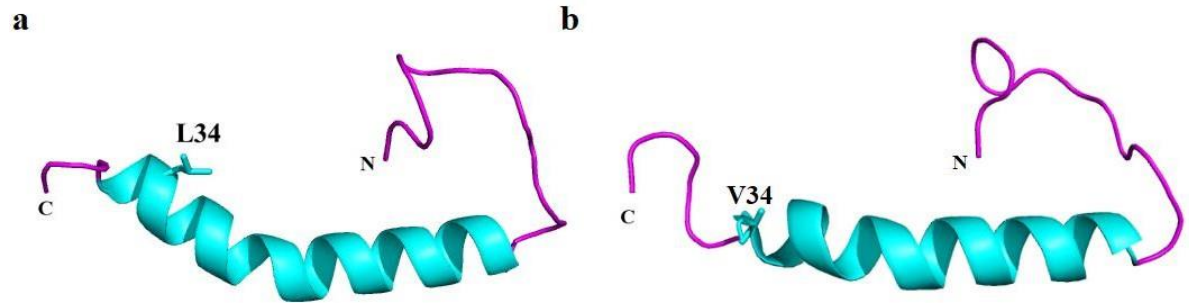

Figure 17: Initial structures of $A\beta_{40}$ and $A\beta_{40}$(L34V) are displayed as a and b, respectively. The side chain of mutated residues L34V is revealed in stick style

3.2 Molecular Dynamics Simulation

Molecular Dynamics Simulations were conducted utilizing GROMACS 5.0 program[44] along with OPLS-AA[45] force field. This force field was utilized due to the fact that the monomer structures (for $A\beta_{40}$ and $A\beta_{42}$) generated by it were considerably identical with the NMR data.[46]

The OPLS-AA force filed has been widely used in many research projects involving study on conformational change of peptides as it provides data in agreement with that of experimental. Nguyen et al. investigated the effect of various force fields on amyloid assembly and stated that OPLS force field predicted diverse conformations (Nguyen et al., 2011)[47]. Sgourakis et al. studied the conformations of Aβ40 and Aβ42 respectively utilizing REMD simulation and various force fields stating OPLS to be efficient enough to produce experimental measurements (Sgourakis et al., 2007).[46] Walter et al. investigated the conformational change of poly(N-isopropylacrylamide) utilizing various force fields and concluded that OPLS was in consent with respect to the experimental results (Walter et al., 2010).[48] Shivakumar et al. examined the solvation free energy using MD simulations along with OPLS force field and found excessive correlation with experimental data (Shivakumar et al., 2010).[49] Several investigations have revealed that OPLS is ideal to scrutinize the accumulation of amyloid β segments in explicit water.[50]

Two explicit-solvent MD simulations were conducted on the systems namely Aβ40 and Aβ40(L34V). Berendsen's coupling algorithm[51] was applied to keep the temperature and pressure constant. In order to constrain the bond lengths LINCS algorithm[52] was utilized with an integration time step of 2 fs. The short–range van der Waals interactions cut–off was fixed at 1.0 nm. Whereas to calculate long–range electrostatic interactions particle mesh Ewald (PME) method[53] was utilized. The system was equilibrated under NVT (constant: number, volume, temperature) conditions for 100 ps at 300 K followed by 100 ps under NPT (constant: number, pressure, temperature) conditions. Each system was subjected to 200 ns simulation and trajectories were sampled at 10 ps interval.

3.3 Trajectory analysis

Analyzation of the simulation trajectories were done utilizing several GROMACS tools along with visual molecular dynamics (VMD)[54] and PyMOL. Clustering of MD ensemble was brought about by employing Daura, et al. algorithm using a cut-off of 0.20 nm over backbone atoms.[55] The structural changes were examined utilizing Root-Mean-Square deviation (RMSD), Radius-of-gyration (R_g) and Root-Mean-Square Fluctuation (RMSF). The Dictionary of secondary structure of proteins (DSSP) was utilized for calculating the secondary structures of $A\beta_{40}$ and $A\beta_{40}$(L34V). The gmx mdmat tool was used for constructing contact map between a pair of residues and the contact maps were visualized utilizing 2D contact maps of all amino acid pairs in contact. The contact frequencies were defined by different colours. The contact

between the two peptide residues is thought to exist when the separation between them is ≤1.5 nm.

Chapter 4

Results and discussion

4.1 Validation of conformational ensemble utilizing NMR data

The accuracy of conformational ensemble obtained by performing MD simulation of 200ns on each system was confirmed by comparing NMR values for the Cα and Cβ atoms, examined by utilizing SHIFTX2 tool (Han et al., 2011)[56] where the experimental NMR values were reported by Hou, et al. (2004).[57] The observed chemical shift values (δ_{sim}) (R = 0.97) for Cα obtained from MD conformational ensemble revealed excellent correlation with experimental chemical shift values (δ_{exp}) of the Cα atoms of $A\beta_{40}$. This correlation is well displayed in Figure 18a. Similarly the observed chemical shift values of the Cβ atoms (R = 0.98) δ_{sim} displayed high quality correlation with δ_{exp} which is well depicted in Figure 18b. The correlation depicted between the theoretical and experimental NMR chemical shift values indicated that molecular dynamics simulations were capable of reproducing the $A\beta_{40}$ structural ensemble reasonably well.

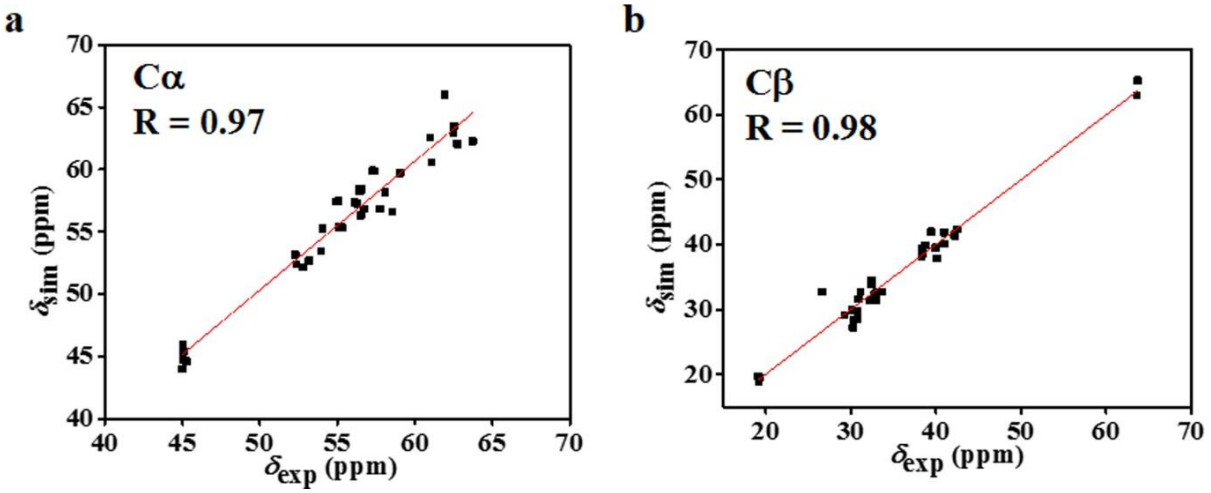

Figure 18: The correlation between simulated and experimental NMR chemical shifts. The correlation for Cα and Cβ atoms of $A\beta_{40}$ are displayed in panel a, and b, respectively. The unit of chemical shift is ppm.

4.2 Conformational behaviour and structural properties of $A\beta_{40}$ and $A\beta_{40}$(L34V)

Clustering analysis of the simulation trajectories were performed which revealed the conformational changes in the respective systems [$A\beta_{40}$ and $A\beta_{40}$(L34V)]. The clustering analysis performed for the MD ensemble was evaluated by comparing macrostates and over the microstates. Evaluation of the conformational microstates which were similar to conformational clusters was done in accordance to Daura et al. (1999) algorithm. The analysis of MD trajectories was based on the comparison in the evolution of number of microstates which were equivalent to the conformational clusters as depicted in Figure 19.

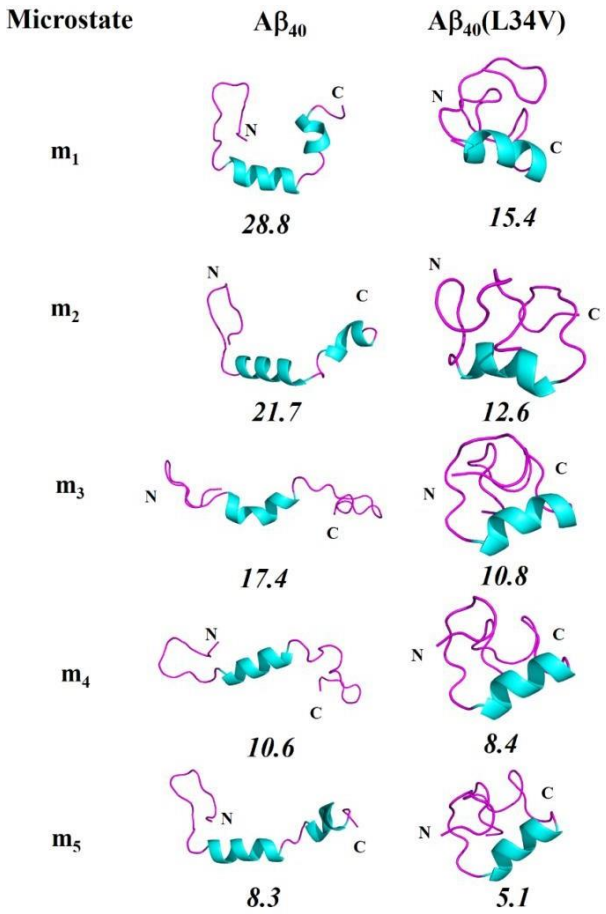

Figure 19: The conformations representing five most-populated microstates (m_1, m_2, m_3, m_4 and m_5) of $A\beta_{40}$ and $A\beta_{40}$(L34V). These are displayed as cartoon representation with N- and C-termini labeled. The percentage population of corresponding microstates is shown underneath.

The models were considered to attain equilibrium and get saturated to distinct populations in the microstates. Clustering of MD trajectories resulted in a total of 67 conformational clusters

for $A\beta_{40}$ in comparison to 98 for $A\beta_{40}$(L34V). The data obtained suggested intensified conformational heterogeneity in $A\beta_{40}$(L34V). Another piece of information achieved from the clustering data was the reduction in percentage population of most-populated microstate. The reduction was considered to be 28.8% for $A\beta_{40}$ to 15.4% for $A\beta_{40}$(L34V). The same was observed for the next four most-populated microstates in which the decrease was from 21.7%, 17.4%, 10.6%, and 8.3% in $A\beta_{40}$ to 12.6%, 10.8%, 8.4%, and 5.1% in $A\beta_{40}$(L34V) stating elevated heterogeneous conformational ensemble for $A\beta_{40}$(L34V).The statistics for the data can be well seen in Table 2

Table 2: The total number of microstates and the percentage population of five most-populated microstates (**m_1**, **m_2**, **m_3**, **m_4** and **m_5**) of $A\beta_{40}$ and $A\beta_{40}$(L34V) during MD simulation in explicit water.

System	Number of microstates	Percentage population of five most-populated microstates				
		m_1	**m_2**	**m_3**	**m_4**	**m_5**
$A\beta_{40}$	67	28.8	21.7	17.4	10.6	8.3
$A\beta_{40}$(L34V)	98	15.4	12.6	10.8	8.4	5.1

In order to examine the relative conformational stability of $A\beta_{40}$ and $A\beta_{40}$(L34V), the Root Mean Square Deviation (RMSD), R_g and Root Mean Square Fluctuations (RMSF) were evaluated (Figure 20). Initially the RMSD fluctuates till ~100 ns followed by attaining equilibrium for both systems (Figure 20a). The data obtained during RMSD fluctuation states lower mean value (~1.04 nm) for Aβ40 in comparison to $A\beta_{40}$(L34V) (~1.13 nm). It was depicted from the data that larger RMSD in $A\beta_{40}$(L34V) compared to $A\beta_{40}$ recommended elevated conformational fluctuations in $A\beta_{40}$. Similarly, the R_g analysis emphasize that in $A\beta_{40}$, the conformations are more compact in comparison to $A\beta_{40}$(L34V) as depicted by lower R_g value. The average value of R_g in $A\beta_{40}$ displays lower value ~1.06 nm as compared to $A\beta_{40}$(L34V) showing ~1.16 nm value illustrating less compact conformation in $A\beta_{40}$(L34V). Figure 20c displays Cα RMSF of $A\beta_{40}$ and $A\beta_{40}$(L34V) . It is depicted from the figure that the residues in N- and C-termini show increased atomic fluctuations in $A\beta_{40}$(L34V) in comparison

to $A\beta_{40}$.The elevated fluctuations of C-terminus residues in $A\beta_{40}$(L34V) illustrate reduced stability of the C-terminal region as compared to $A\beta_{40}$.

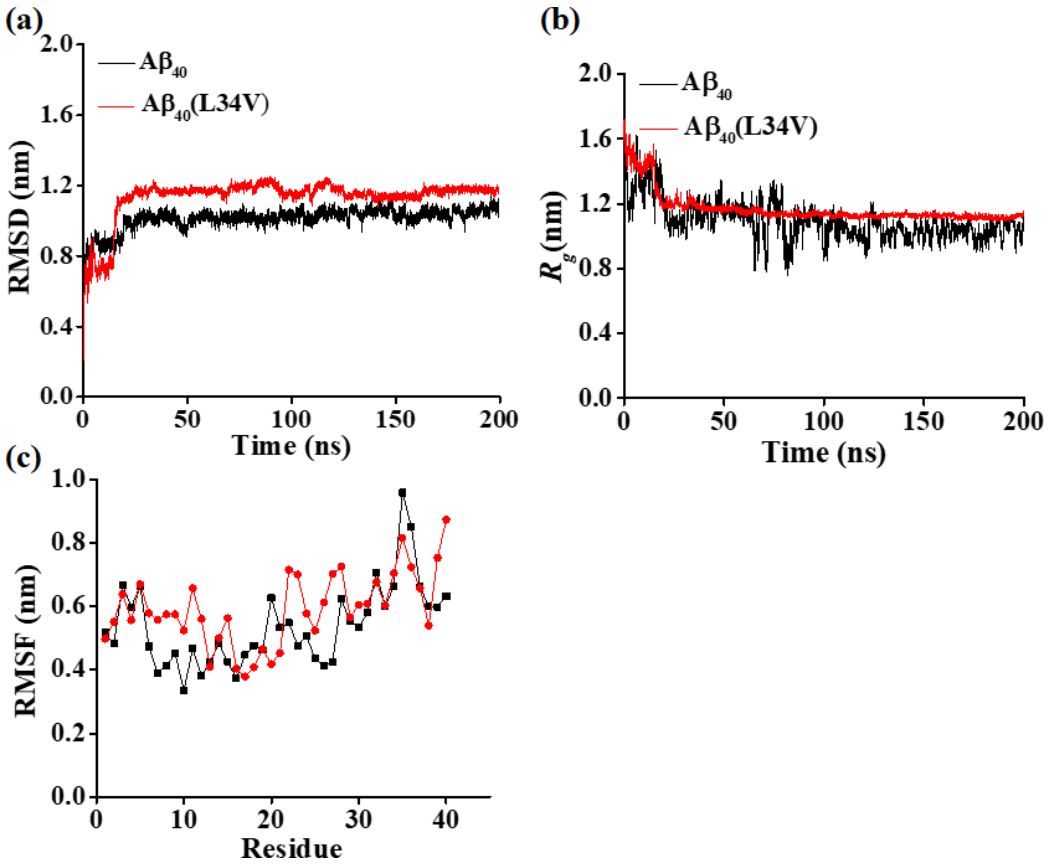

Figure 20: Showing RMSD, R_g and RMSF data. The Root-Mean-Square Deviation, RMSD (panel a) and Radius-of-gyration, R_g, (panel b) are plotted as a function of simulation time in ns. The Root-Mean-Square Fluctuations (RMSF) of each residue in $A\beta_{40}$ and $A\beta_{40}$(L34V) is shown in panel c.

4.3 Impact of L34V mutation on the secondary structure of $A\beta_{40}$

Statistically stating the percentage for Aβ40 of coil, β–sheet, helix, bend, and turn content is 50%, 1%, 19%, 12%, and 18%, respectively displayed in Table 3. The dominance of coil and turn conformation in $A\beta_{40}$ is in agreement with earlier results.[58] The C-terminal of Aβ40 comprises of higher β-sheet content at the residues 33-37 whereas the CHC region (16-21) is restricted to the α-helical structure through the initial 170 ns. Afterward it shows irregular local deviations from α-helix to coil or bend conformations. Throughout the simulation the N-terminal residues in the region 5-10 chiefly adopt a random coil conformation during the

simulation. MD simulation results of Aβ40 showing relatively poor β-sheet structure are in agreement with a number of studies.[59]

Table 3: Statistical representation of secondary structure components of $A\beta_{40}$ and $A\beta_{40}$(L34V) during Molecular Dynamics Simulation in water as explicit-solvent.

model system	coil	β-sheet[a]	helix[b]	bend	turn
$A\beta_{40}$	50	1	19	12	18
$A\beta_{40}$(L34V)	38	3	13	10	36

[a]β–sheet is the sum of β–sheet and β-bridge; [b]helix is the sum of α–, π– and 3_{10} helix

In case of $A\beta_{40}$(L34V), the percentage of coil, β–sheet, helix, bend, and turn content is 38%, 3%, 13%, 10%, and 36%, respectively (Table 3). From the data mentioned in Table 3 it can be well depicted that there is a reduction in coil conformation at the C-terminal region displaying turn conformation throughout simulation (Figure 21, lower panel). Upon L34V mutation, the β–content and turn content elevates from 1% in $A\beta_{40}$ to 3% and 18% to 36% in $A\beta_{40}$(L34V). Thus, in agreement with the experimental results, L34V mutation in $A\beta_{40}$ is capable of elevating the β–sheet content and aggregation prone turn conformation, which exaggerates the aggregation of $A\beta_{40}$. The reduction in helix percentage from 19% in $A\beta_{40}$ to 13% in $A\beta_{40}$(L34V) is also in support with the experimental evidence stating lower helix content for $A\beta_{40}$(L34V) as compared to $A\beta_{40}$. The secondary structure analysis emphasize that L34V mutation considerably affected the overall content of α–helix, β–sheet, turn, bend, and coil conformations in $A\beta_{40}$.

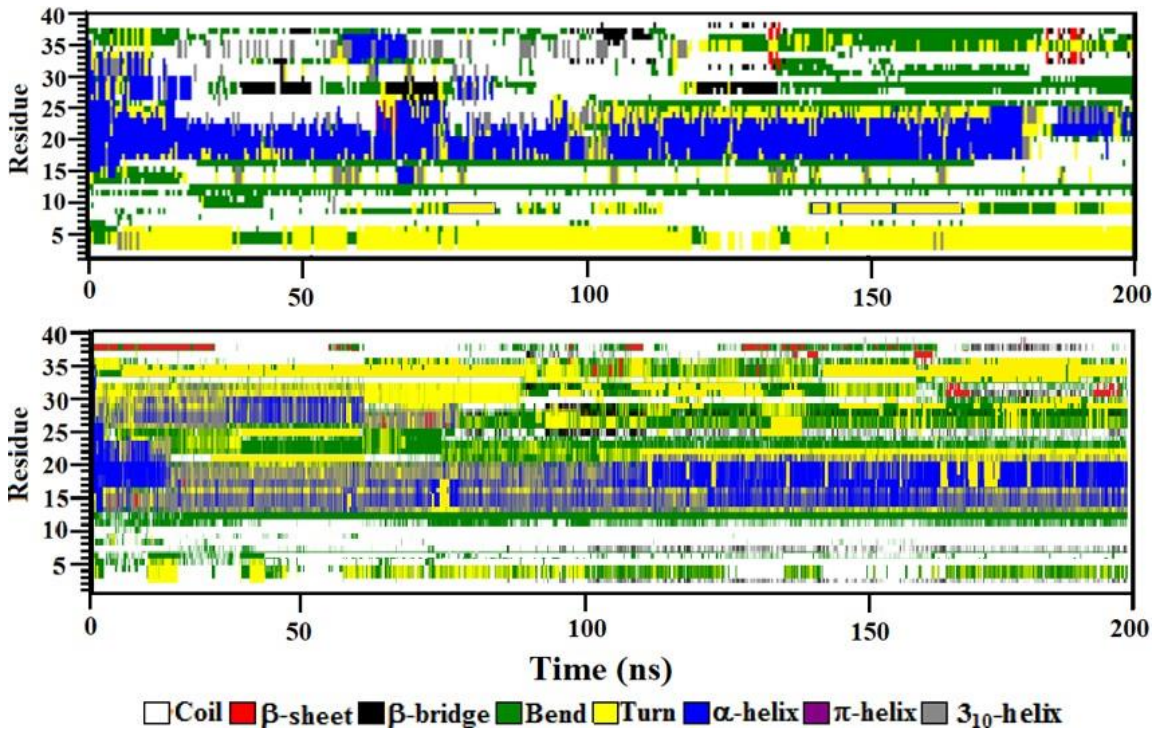

Figure 21: The evolution of secondary structure component as a function of simulation time (ns). The data is represented for $A\beta_{40}$ and $A\beta_{40}$(L34V) in upper and lower panel, respectively. The secondary structure components are colour coded as shown underneath.

4.4 Impact of L34V mutation on the tertiary structure

Several experimental and theoretical researches are known to report the interactions between CHC and C-terminal region showing significant role in early $A\beta_{40}$ folding and self-assembly (Scira and co-workers).[60] However, increase in intramolecular interaction between CHC and C-terminal region would promote $A\beta_{40}$ folding and self-aggregation.[61] Taking into consideration both the systems i.e. Aβ40 and L34V, it was observed that in case of $A\beta_{40}$ high profuse short-range interactions between residues spanning CHC and mid-domain/C–terminal region (within 1.5 nm distance between side chain atoms) were prevalent (Figure 21a).Whereas considering $A\beta_{40}$(L34V) it was found that there was an increase in intramolecular tertiary contacts between CHC and C-terminus (Figure 21b). Overall these results indicated that L34V residue played a central role in forming long range and short range intramolecular interactions in $A\beta_{40}$.The replacement of L34 with valine, resulted in an increase in the probability of forming short range contacts in $A\beta_{40}$(L34V). The overall elevation in intrapeptide contacts clearly indicate higher probability of $A\beta_{40}$folding and self-assembly upon L34V mutation.

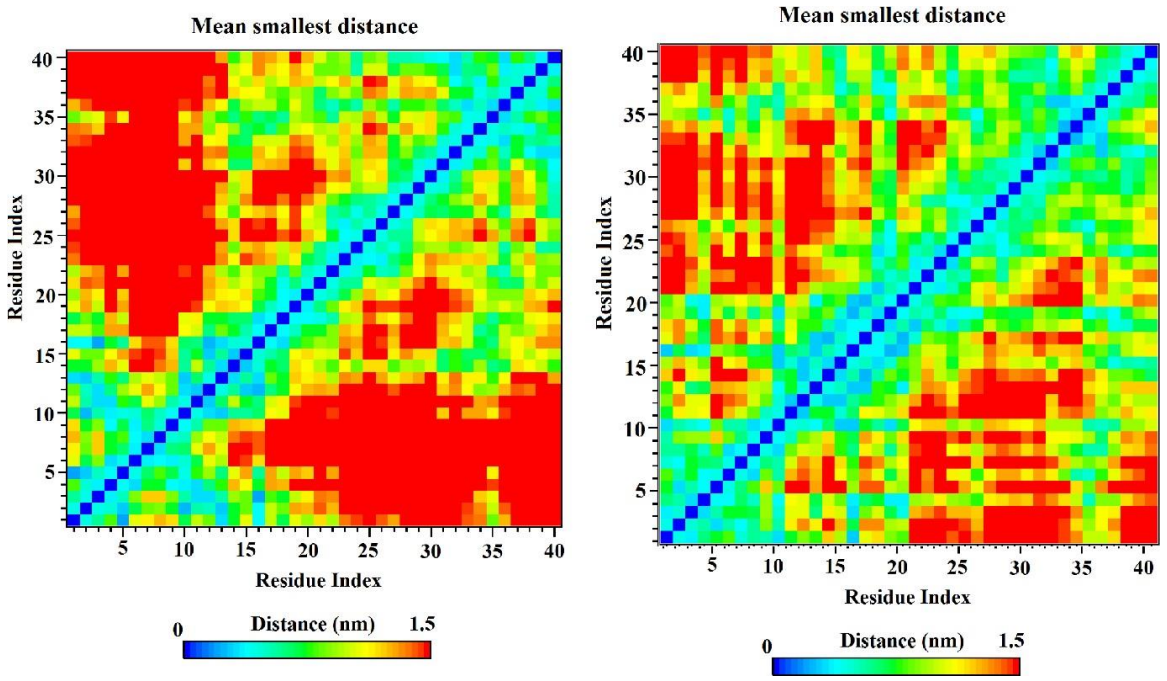

Figure 22: The intrapeptide side chain contacts in Aβ$_{40}$ and Aβ$_{40}$(L34V). The analysis is displayed in panel a, and b, respectively. The colour scale corresponds to the distance between the side chain atoms being ≤1.5 nm from each other.

4.5 Hydrophobic and hydrophilic SASA of Aβ$_{40}$ and Aβ$_{40}$(L34V)

It is well known that the detection and assembly of amyloid fibrils is initiated by an exposed hydrophobic surface of residues.[62] Several studies reported that the stabalization of β–sheets and helices is due to the hydrophobic effect and hydrophilicity respectively. In the present study we have calculated hydrophobic and hydrophilic solvent accessible surface area (SASA) of Aβ$_{40}$ and Aβ$_{40}$(L34V) as shown in Figure 22.

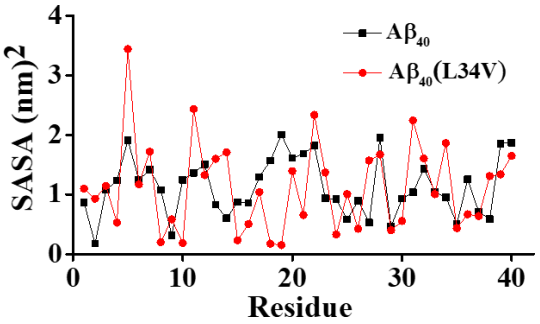

Figure 23: The solvent accessible surface area (SASA) of each residue in Aβ$_{40}$ and Aβ$_{40}$(L34V).

The data obtained stated that the SASA of residues at C-terminal was particularly elevated in $A\beta_{40}$(L34V) in comparison to $A\beta_{40}$. This higher SASA of C-terminal region suggested that the residues of C-terminal were exposed to the solvent. Generally the stability of $A\beta_{40}$ monomer is evaluated, in terms of SASA, by reduction in the region for hydrophobic residues and elevation in the region for hydrophilic residues. The elevated SASA values in C-terminal area suggest that the residues in this area have higher tendencies to aggregate and self-assemble.[63] Therefore, $A\beta_{40}$(L34V) mutation is capable of enhancing $A\beta_{40}$ aggregation by exposing the solvent exposed region of residues in C-terminal residues.

Chapter 5

Conclusions

Using all-atom molecular dynamics simulations, we investigated the influence of L34V mutation on the structure, dynamics and conformation of $A\beta_{40}$. The present study highlight that L34V mutation results in increase in aggregation propensity of $A\beta_{40}$ by inducing conformational fluctuations as depicted by conformational clustering analysis, RMSD, RMSF, R_g values and analysis of secondary structure content of $A\beta_{40}$. The reduction in the percentage population of most populated microstate from $A\beta_{40}$ to $A\beta_{40}$(L34V)as observed in the clustering analysis highlight conformational heterogeneity on L34V mutation. The RMSF values indicated elevated fluctuations in C-terminus upon L34V mutation, which lead to decrease in the stability of C- terminus of $A\beta_{40}$. The secondary structure analysis of $A\beta_{40}$ highlights marginal increase in the β-sheet content and a decrease in the helical conformation from 19% to 13%. The L34V mutation lead to an increase in the intrapeptide short range contacts, which depict higher aggregation propensity for the $A\beta_{40}$(L34V) as compare to wt-$A\beta_{40}$. The SASA analysis highlight enhanced SASA values of the C-terminus, which suggest that residues in this region has high aggregation propensity. The present study provided structural and mechanistic details into the effect of L34V mutation on the structure and dynamics of $A\beta_{40}$, which will further aid in a better understanding of the molecular mechanism of the AD.

References

1. Nölting, B.; Andert, K. Mechanism of protein folding. *Proteins: Struct. Funct. Bioinf.,* **2000**, *41*, 288-298.

2. a) Bryngelson, J. D., Onuchic, J. N., Socci, N. D., & Wolynes, P. G. Funnels, pathways, and the energy landscape of protein folding: a synthesis. *Proteins: Struct. Funct. Bioinf.,* **1995**, *21*, 167-195; b) Onuchic, J. N., Luthey-Schulten, Z., & Wolynes, P. G. Theory of protein folding: the energy landscape perspective. *Annu. Rev. Phys. Chem.,* **1997**, *48*, 545-600.

3. Chaudhuri, T. K.; Paul, S. Protein-misfolding diseases and chaperone-based therapeutic approaches. *FEBS J.,* **2006**, *273*, 1331-1349.

4. Dobson, C. M. Protein folding and misfolding. *Nature*, **2003**, *426*, 884.

5. Neugroschl, J., & Sano, M. Current treatment and recent clinical research in Alzheimer's disease. *Mt. Sinai. J. Med.*, **2010**, *77*, 3-16.

6. Chuang, E.; Hori, A. M.; Hesketh, C. D.; Shorter, J. Amyloid assembly and disassembly. *J. Cell. Sci.,* **2018**, *131*, doi: 10.1242/jcs.189928.

7. Fitzpatrick, A. W., Falcon, B., He, S., Murzin, A. G., Murshudov, G., Garringer, H. J., & Scheres, S. H. Cryo-EM structures of tau filaments from Alzheimer's disease. *Nature*, **2017**, *547*, 185.

8. Sgarbossa, A. Natural biomolecules and protein aggregation: emerging strategies against amyloidogenesis. *Int. J. Mol. Sci.*, **2012**, *13*, 17121-17137.

9. Cai, Y.; An, S. S. A.; Kim, S. Mutations in presenilin 2 and its implications in Alzheimer's disease and other dementia-associated disorders. *Clin. Interv. Aging.*, **2015**, *10*, 1163.

10. Hardy, J. A., & Higgins, G. A. Alzheimer's disease: the amyloid cascade hypothesis. *Science* **1992**, *256*, 184.

11. Selkoe, D. J., & Hardy, J. The amyloid hypothesis of Alzheimer's disease at 25 years. *EMBO Mol. Med.,* **2016**, *8*, 595-608.

12. Ono, K., Condron, M. M., & Teplow, D. B. Structure–neurotoxicity relationships of amyloid β-protein oligomers. *Proc. Natl. Acad. Sci.,* **2009**, *106*, 14745-14750.

13. Sarell, C. J., Wilkinson, S. R., & Viles, J. H. Sub-stoichiometric levels of $Copper^{2+}$ ions accelerate the kinetics of fibre formation and promote cell toxicity of amyloid-beta from Alzheimer's disease. *J. Biol. Chem.,* **2010**, jbc-M110.

14. Zlokovic, B. V. New therapeutic targets in the neurovascular pathway in Alzheimer's disease. *Neurotherapeutics,* **2008**, *5*, 409-414.

15. Ferreira, L. G.; dos Santos, R. N.; Oliva, G.; Andricopulo, A. D. Molecular docking and structure-based drug design strategies. *Molecules*, **2015**, *20*, 13384-13421.

16. Durrant, J. D.; McCammon, J. A. Molecular dynamics simulations and drug discovery. *BMC Biol.*, **2011**, *9*, 71.

17. Das, P.; Murray, B.; Belfort, G. Alzheimer's protective A2T mutation changes the conformational landscape of the Aβ1–42 monomer differently than does the A2V mutation. *Biophys. J.,* **2015**, *108*, 738-747.

18. Giaccone, G.; Morbin, M.; Moda, F.; Botta, M.; Mazzoleni, G.; Uggetti, A.; Catania, M.; Moro, M. L.; Redaelli, V.; Spagnoli, A. Neuropathology of the recessive A673V APP mutation: Alzheimer disease with distinctive features. *Acta neuropathol.,* **2010**, *120*, 803-812.

19. Ono, K.; Condron, M. M.; Teplow, D. B. Effects of the English (H6R) and Tottori (D7N) familial Alzheimer disease mutations on amyloid β-protein assembly and toxicity. *J. Biol. Chem.,* **2010,** *285*, 23186-23197.

20. Xu, L.; Chen, Y.; Wang, X. Dual effects of familial Alzheimer's disease mutations (D7H, D7N, and H6R) on amyloid β peptide: Correlation dynamics and zinc binding. Proteins: Struct. Funct. Bioinf., **2014**, *82*, 3286-3297.

21. Viet, M. H.; Nguyen, P. H.; Ngo, S. T.; Li, M. S.; Derreumaux, P. Effect of the Tottori Familial Disease Mutation (D7N) on the Monomers and Dimers of Aβ40 and Aβ42. *ACS Chem. Neurosci.,* **2013**, *4*, 1446-1457.

22. Kaden, D.; Harmeier, A.; Weise, C.; Munter, L. M.; Althoff, V.; Rost, B. R.; Hildebrand, P. W.; Schmitz, D.; Schaefer, M.; Lurz, R. Novel APP/Aβ mutation K16N produces highly toxic heteromeric Aβ oligomers. *EMBO Mol. Med.*, **2012**, *4*, 647-659.

23. Rodziewicz-Motowidło, S.; Juszczyk, P.; Kołodziejczyk, A. S.; Sikorska, E.; Skwierawska, A.; Oleszczuk, M.; Grzonka, Z. Conformational solution studies of the SDS micelle-bound 11-28 fragment of two Alzheimer's β-amyloid variants (E22K and A21G) using CD, NMR, and MD techniques. *Biopolymers*, **2007**, *87*, 23-39.

24. Jang, H.; Teran Arce, F.; Ramachandran, S.; Kagan, B. L.; Lal, R.; Nussinov, R. Familial Alzheimer's disease Osaka mutant (ΔE22) β-barrels suggest an explanation for the different Aβ1–40/42 preferred conformational states observed by experiment. *J. Phys. Chem., B* **2013,** *117*, 11518-11529.

25. Bossis, F.; Palese, L. L. Amyloid beta (1–42) in aqueous environments: effects of ionic strength and E22Q (Dutch) mutation. *Biochim. Biophys. Acta.*, **2013**, *1834*, 2486-2493.

26. Blinov, N.; Dorosh, L.; Wishart, D.; Kovalenko, A. Association thermodynamics and conformational stability of β-sheet amyloid β (17-42) oligomers: Effects of E22Q (Dutch) mutation and charge neutralization. *Biophys. J.*, **2010**, *98*, 282-296.

27. Xu, L.; Shan, S.; Wang, X. Single point mutation alters the microstate dynamics of amyloid β-protein Aβ42 as revealed by dihedral dynamics analyses. *J. Phys. Chem., B* **2013**, *117*, 6206-6216.

28. Nilsberth, C.; Westlind-Danielsson, A.; Eckman, C. B.; Condron, M. M.; Axelman, K.; Forsell, C.; Stenh, C.; Luthman, J.; Teplow, D. B.; Younkin, S. G. The 'Arctic' APP mutation (E693G) causes Alzheimer's disease by enhanced Aβ protofibril formation. *Nat. Neurosci.*, **2001**, *4*, 887.

29. Okamoto, A.; Yano, A.; Nomura, K.; Higai, S. I.; Kurita, N. Effect of D23N mutation on the dimer conformation of amyloid β-proteins: Aβ initio molecular simulations in water. *J. Mol. Graphics Model.*, **2014**, *50*, 113-124.

30. Van Nostrand, W. E.; Melchor, J. P.; Cho, H. S.; Greenberg, S. M.; Rebeck, G. W. Pathogenic effects of D23N Iowa mutant amyloid β-protein. *J. Biol. Chem.*, **2001**, *276*, 32860-32866.

31. Argyri, L.; Dafnis, I.; Theodossiou, T. A.; Gantz, D.; Stratikos, E.; Chroni, A. Molecular basis for increased risk for late-onset Alzheimer disease due to the naturally occurring L28P mutation in apolipoprotein E4. *J. Biol. Chem.*, **2014**, *289*, 12931-12945.

32. Subramanian, S.; Mishra, P. K.; Bandopadhyay, D. I32E and V36K double mutation in beta2-sheet abrogates amyloid beta peptide toxicity. *Indian J. Exp. Biology*, **2010**, *48*, 1098-1102.

33. Liang, C.-T.; Huang, H.-B.; Wang, C.-C.; Chen, Y.-R.; Chang, C.-F.; Shiao, M.-S.; Chen, Y.-C.; Lin, T.-H. L17A/F19A substitutions augment the α-helicity of β-amyloid peptide discordant segment. *PloS One* **2016**, *11*, e0154327.

34. Rodziewicz-Motowidło, S.; Wahlbom, M.; Wang, X.; Łągiewka, J.; Janowski, R.; Jaskólski, M.; Grubb, A.; Grzonka, Z. Checking the conformational stability of cystatin C and its L68Q variant by molecular dynamics studies: Why is the L68Q variant amyloidogenic? *J. Struct. Biol.*, **2006**, *154*, 68-78.

35. Shimojo, M.; Sahara, N.; Mizoroki, T.; Funamoto, S.; Morishima-Kawashima, M.; Kudo, T.; Takeda, M.; Ihara, Y.; Ichinose, H.; Takashima, A. Enzymatic Characteristics of I213T Mutant Presenilin-1/γ-Secretase in Cell Models and Knock-in Mouse Brains familial Alzheimer disease linked mutation impairs γ-site cleavage of amyloid precursor protein C terminal fragment β. *J. Biol. Chem.*, **2008**, *283*, 16488-16496.

36. Korn, A.; McLennan, S.; Adler, J.; Krueger, M.; Surendran, D.; Maiti, S.; Huster, D. Amyloid β (1-40) Toxicity Depends on the Molecular Contact Between Phenylalanine 19 and Leucine 34. *ACS Chem. Neurosci.*, **2017**, DOI: 10.1021/acschemneuro.7b00360.

37. Obici, L.; Demarchi, A.; de Rosa, G.; Bellotti, V.; Marciano, S.; Donadei, S.; Arbustini, E.; Palladini, G.; Diegoli, M.; Genovese, E. A novel AβPP mutation exclusively associated with cerebral amyloid angiopathy. *Ann. Neurol.*, **2005**, *58*, 639-644.

38. Fossati, S.; Cam, J.; Meyerson, J.; Mezhericher, E.; Romero, I.; Couraud, P.; Weksler, B.; Ghiso, J.; Rostagno, A. Differential activation of mitochondrial apoptotic pathways by vasculotropic amyloid-β variants in cells composing the cerebral vessel walls. *FASEB J.*, **2010**, *24*, 229-241.

39. Hernandez-Guillamon, M.; Mawhirt, S.; Fossati, S.; Blais, S.; Pares, M.; Penalba, A.; Boada, M.; Couraud, P.-O.; Neubert, T. A.; Montaner, J. Matrix metalloproteinase 2 (MMP-2) degrades soluble vasculotropic amyloid-β E22Q and L34V mutants, delaying their toxicity for human brain microvascular endothelial cells. *J. Biol. Chem.*, **2010**, *285*, 27144-27158.

40. Hatami, A.; Monjazeb, S.; Milton, S.; Glabe, C. G. Familial Alzheimer's Disease Mutations within the Amyloid Precursor Protein Alter the Aggregation and Conformation of the Amyloid-β Peptide. *J. Biol. Chem.*, **2017**, *292*, 3172-3185.

41. Panda, P. K.; Patil, A. S.; Patel, P.; Panchal, H. Mutation-based structural modification and dynamics study of amyloid beta peptide (1–42): An in-silico-based analysis to cognize the mechanism of aggregation. *Genom. Data*, **2016**, *7*, 189-194.

42. Coles, M.; Bicknell, W.; Watson, A. A.; Fairlie, D. P.; Craik, D. J. Solution Structure of Amyloid β-Peptide (1− 40) in a Water-Micelle Environment. Is the Membrane Spanning Domain Where We Think It Is? *Biochemistry* **1998**, *37*, 11064-11077.

43. DeLano, W. The PyMOL Molecular Graphics System. San Carlos, CA: DeLano Scientific; **2002**.

44. Abraham, M. J.; Murtola, T.; Schulz, R.; Páll, S.; Smith, J. C.; Hess, B.; Lindahl, E. GROMACS: High performance molecular simulations through multi-level parallelism from laptops to supercomputers. *SoftwareX*, **2015**, *1*, 19-25.

45. Jorgensen, W. L.; Maxwell, D. S.; Tirado-Rives, J. Development and testing of the OPLS all-atom force field on conformational energetics and properties of organic liquids. *J. Am. Chem. Soc.*, **1996**, *118*, 11225-11236.

46. Sgourakis, N. G.; Yan, Y.; McCallum, S. A.; Wang, C.; Garcia, A. E. The Alzheimer's peptides Aβ40 and 42 adopt distinct conformations in water: a combined MD/NMR study. *J. Mol. Biol.*, **2007**, *368*, 1448-1457.

47. Nguyen, P. H., Li, M. S., & Derreumaux, P. Effects of all-atom force fields on amyloid oligomerization: Replica exchange molecular dynamics simulations of the Aβ 16–22 dimer and trimer. *Phys. Chem. Chem. Phys.*, **2011**, *13*, 9778-9788.

48. Walter, J., Ermatchkov, V., Vrabec, J., & Hasse, H. Molecular dynamics and experimental study of conformation change of poly (N-isopropylacrylamide) hydrogels in water. *J. Fluid Phase Equilib.,* **2010**, *296,* 164-172.

49. Shivakumar, D., Williams, J., Wu, Y., Damm, W., Shelley, J., & Sherman, W. Prediction of absolute solvation free energies using molecular dynamics free energy perturbation and the OPLS force field. *J. Chem. Theory. Comput.,* **2010,** *6,* 1509-1519.

50. Nguyen, P. H.; Li, M. S.; Derreumaux, P. Effects of all-atom force fields on amyloid oligomerization: Replica exchange molecular dynamics simulations of the Aβ 16–22 dimer and trimer. *Phys. Chem. Chem. Phys.,* **2011**, *13,* 9778-9788.

51. Van Gunsteren, W. F.; Berendsen, H. A leap-frog algorithm for stochastic dynamics. *Mol. Simulat.,* **1988,** *1*, 173-185.

52. Hess, B.; Bekker, H.; Berendsen, H. J.; Fraaije, J. G. LINCS: a linear constraint solver for molecular simulations. *J. Comp. Chem.,* **1997**, *18,* 1463-1472.

53. Darden, T.; York, D.; Pedersen, L. Particle mesh Ewald: An N· log (N) method for Ewald sums in large systems. *The J. Chem. Phys.,* **1993**, *98,* 10089-10092.

54. Humphrey, W.; Dalke, A.; Schulten, K. VMD: visual molecular dynamics. *J. Mol. Graph.,* **1996**, *14,* 33-38.

55. Daura, X.; Gademann, K.; Jaun, B.; Seebach, D.; Van Gunsteren, W. F.; Mark, A. E. Peptide folding: when simulation meets experiment. *Angew. Chem. Int. Ed.,* **1999**, *38*, (1-2), 236-240.

56. Han, B., Liu, Y., Ginzinger, S. W., & Wishart, D. S. SHIFTX2: significantly improved protein chemical shift prediction. *J. Biomol. NMR.,* **2011**, *50,* 43.

57. Hou, L., Shao, H., Zhang, Y., Li, H., Menon, N. K., Neuhaus, E. B., & Iwashita, T. Solution NMR studies of the Aβ (1− 40) and Aβ (1− 42) peptides establish that the Met35 oxidation state affects the mechanism of amyloid formation. *J. Am. Chem. Soc.,* **2004**, *126,* 1992-2005.

58. Truong, P. M.; Viet, M. H.; Nguyen, P. H.; Hu, C.-K.; Li, M. S. Effect of Taiwan Mutation (D7H) on Structures of Amyloid-β Peptides: Replica Exchange Molecular Dynamics Study. *J. Phys. Chem., B* **2014**, *118*, 8972-8981.

59. Viet, M. H.; Nguyen, P. H.; Derreumaux, P.; Li, M. S. Effect of the English Familial Disease Mutation (H6R) on the Monomers and Dimers of Aβ40 and Aβ42. *ACS Chem. Neurosci.*, **2014**, *5*, 646-657.

60. Wise-Scira, O., Xu, L., Perry, G., & Coskuner, O. Structures and free energy landscapes of aqueous zinc (II)-bound amyloid-β (1–40) and zinc (II)-bound amyloid-β (1–42) with dynamics. *J. Biol. Inorg. Chem.*, **2012**, *17*, 927-938.

61. Coskuner, O.; Wise-Scira, O., Arginine and Disordered Amyloid-β Peptide Structures: Molecular Level Insights into the Toxicity in Alzheimer's Disease. *ACS Chem. Neurosci.*, **2013**, *4*, 1549-1558.

62. Berhanu, W. M.; Masunov, A. E., Molecular dynamic simulation of wild type and mutants of the polymorphic amyloid NNQNTF segments of elk prion: Structural stability and thermodynamic of association. *Biopolymers*, **2011**, *95*, 573-590.

63. Senguen, F. T.; Doran, T. M.; Anderson, E. A.; Nilsson, B. L. Clarifying the influence of core amino acid hydrophobicity, secondary structure propensity, and molecular volume on amyloid-β 16–22 self-assembly. *Mol. BioSyst.*, **2011**, *7*, 497-510.

Thesis3

ORIGINALITY REPORT

15%	9%	14%	%
SIMILARITY INDEX	INTERNET SOURCES	PUBLICATIONS	STUDENT PAPERS

PRIMARY SOURCES

1	www.jbc.org Internet Source	2%
2	pubs.acs.org Internet Source	2%
3	Suniba Shuaib, Bhupesh Goyal. " Scrutiny of the mechanism of small molecule inhibitor preventing conformational transition of amyloid-β monomer: insights from molecular dynamics simulations ", Journal of Biomolecular Structure and Dynamics, 2017 Publication	1%
4	www.cell.com Internet Source	1%
5	Pritam Kumar Panda, Abhaysinha Satish Patil, Priyam Patel, Hetalkumar Panchal. "Mutation-based structural modification and dynamics study of amyloid beta peptide (1–42): An in - silico-based analysis to cognize the mechanism of aggregation", Genomics Data, 2016 Publication	1%

Bhupesh Goyal H Thakur